ELECTRONIC, SPINTRONIC AND TRANSPORT PROPERTIES OF CARBON BASED NANOWIRES

A Thesis Submitted to
the Graduate School of Engineering and Sciences of
İzmir Institute of Technology
in Partial Fulfillment of the Requirements for the Degree of

MASTER OF SCIENCE

in Physics

by
Ozan ARI

July 2011
IZMIR

We approve the thesis of **Ozan ARI**

Assoc. Prof. Dr. Ramazan Tuğrul SENGER
Supervisor

Prof. Dr. Nejat BULUT
Committee Member

Prof. Dr. İsmail SÖKMEN
Committee Member

07 July 2011

Prof. Dr. Nejat BULUT
Head of the Department of
Physics

Prof. Dr. Durmuş Ali DEMİR
Dean of the Graduate School of
Engineering and Sciences

ACKNOWLEDGMENTS

When I open someones thesis, the first part I read is the acknowledgement. It gives me an insight on the personality of the author. During my time as a M.Sc. student, I have been positively influenced by many, and I am afraid I will not be able to thank everyone properly.

First of all, I would like to express my sincere gratitude to Assoc. Prof. Dr. Ramazan Tuğrul Senger for giving me the opportunity to work as his student. Over the course of this thesis, he has always been willing to listen to any problem and to provide helpful suggestions and comments. Without his guidance and patience, this thesis would not exist in this form.

I think it is important to feel comfortable in a working space, since you spend a big part of the day there. I can ensure, that this work would have been much more of a struggle if it would not have been for the nice environment in the office. For this, I thank to Cihan Bacaksız, Onur Tosun and Oktay Doğangün for their friendship, support, and fruitful discussions. And also I thank to all friends at Izmir Institute of Technology (IYTE) for their friendship.

Next, I would like to thank my parents for all the encouragement and support throughout my whole life. Thanks for putting up with me, taking care of me and raising me the way you have done. I hope you have done a good job. I can not imagine the suffer you have gone through and the sacrifices you have made, so my siblings and I can have this life. Thank you.

Last, but certainly not least, I want to thank my wife. Thank you Özge for your endless support, for the joy we have already had together and the great future that lies ahead of us!

ABSTRACT

ELECTRONIC, SPINTRONIC AND TRANSPORT PROPERTIES OF CARBON BASED NANOWIRES

In this thesis, properties of carbon based nanowires are studied by ab-initio calculations. The aim is to gain a thorough understanding of the electronic, spintronic, transport properties in nanowires and how they are affected by different geometric formations, defects and adatom adsorptions. To this end the non-equilibrium Green's function formalism with first principles pseudopotential density functional theory calculations have been used to describe spin-polarized systems. Firstly, different geometric formations of Cobalt-Benzene nanowires are investigated. Systems with ferromagnetic ordering are calculated as half-metallic while systems with antiferromagnetic ordering behave as metallic. Also the results of the spin polarized current calculations indicate that one of the spin components of current is dominant for the antiferromagnetic systems while both spin components of current are dominant in different bias windows of a specific total applied bias. As second case, alkali atom termination of the zigzag graphene nanoribbons (ZGNR) are studied. In particular, using sodium atoms for the saturation of ZGNR edges at half the concentration of edge-carbon atoms make it a one dimensional, perfect semimetal, where the valance and conduction bands meet at only a single, Dirac-like point. Unlike pristine graphene, the Dirac-"cones" of Na-ZGNR is not symmetric with respect to wave vector, but rather it is tilted. Finally, adsorption up to the graphenic sheets with periodic 5-8 defects is studied. Especially, electronic structure of the V adsorption into 5-8 defects induced graphenic sheets are calculated as half-metallic while formation of linear bands crossing at the Fermi level which form a tilted Dirac cone.

ÖZET

KARBON BAZLI NANOTELLERİN ELEKTRONİK, SPİNTRONİK VE TRANSPORT ÖZELLİKLERİ

Bu tezde, karbon bazlı nano tellerin özellikleri temelden (ab-initio) hesaplamalarla çalışılmıştır. Amaç, nanotellerin elektronik, spintronik ve taşınım özelliklerini ve bu özelliklerin farklı geometrik oluşumlar ve kusurlardan nasıl etkilendiğini anlamaktır. Bu bağlamda spin polarizasyonlu sistemler, dengede dışı Green fonksiyonu formalizmiyle temelden psödopotansiyel yoğunluk fonksiyonel teorisi hesaplamaları kullanılarak belirtilmiştir. İlk olarak, Kobalt-Benzen nano tellerinin farklı geometrik oluşumları incelenmiştir. Anti-ferromanyetik sistemler metal olarak davranırken, ferromanyetik dizilime sahip sistemler yarı-metal olarak hesaplanmıştır. Ayrıca spin polarizasyonlu akım hesaplarının sonuçları, uygulanan bir voltaj aralığında, anti-ferromanyetik sistemlerde sadece bir spin bileşenin baskın olduğunu gösterirken ferromanyetik sistemlerde farklı voltaj aralıklarında farklı spin bileşenlerinin baskın olduğunu göstermektedir. İkinci durum olarak, zigzag grafin nano şeritlerinin (ZGNŞ) alkali atomlarla sonlandırılması çalışılmıştır. Özellikle, ZGNŞ'nin, kenar karbon atomlarının yarı konsantrasyonunda sodyum ile sonlandırılması (Na-ZGNŞ) değerlik ve iletim bantlarının tek bir Dirac-benzeri noktada kesişmesine ve sistemin tek boyutlu, mükemmel bir semi-metal olmasını sağlamıştır. Saf grafinin aksine, Na-ZGNŞ'nin Dirac-"konileri" dalga vektörüne göre simetrik değildir ve eğilmiştir. Son olarak da, 5-8 kusurları oluşturulmuş grafenik katmanların üzerine atom emilimi çalışılmıştır. Bilhassa, vanadyum atomunun 5-8 kusurlarına sahip grafenik katmanlar üzerine emiliminde elektronik yapı, lineer bantların Fermi seviyesinde eğimli bir Dirac konisi oluşturacak şekilde ve yarı metal olarak hesaplanmıştır.

TABLE OF CONTENTS

LIST OF FIGURES

LIST OF TABLES

CHAPTER 1

INTRODUCTION

Semiconductor materials changed the modern electronics completely during the second half of the last century. Scientific and technologic improvements in electronics have created new possibilities in the communication and information processing areas which lead to invention of computers and communication devices such as mobile phones. Small devices like silicon chips, which contain lots of components, became producible with the invention of solid state transistor and the integrated circuit(IC). An IC is an electronic circuit where all electronic components (transistors, capacitors, interconnects) are integrated on a single silicon chip. The increase in the efficiency of integrated circuits allowed having more components in the silicon chips. In 1965 Gordon E. Moore predicted that the number of the transistors on a chip would double every year [1]. However Moore's prediction was for only ten years. The doubling of the number of transistors is approximately every 18 months. The performance of electronic devices always increased with the tuning down the systems. Today a high-end computer processor contains a few billion transistors. Although this exponential growth must end at the point which quantum mechanical effects such as Heisenberg uncertainty principle [2, 3] or other effects such as electro-migration process [4] and subthreshold leakage currents between electrodes of transistor [5] become disturbing factor in electronic device design. Approximately two more decades [6, 7] will be the limit of scaling in conventional semiconductor material. Radically different approaches for future electronic devices are needed. Spintronics and molecular electronics are the two most promising approaches for the problem.

Placing an electron in a magnetic field results in a coupling of its magnetic moment to the magnetic field. Now if the spin of an electron is measured along a certain axis, one may obtain only two possible results which are spin-up or spin-down states. This property of electron can be used to perform Boolean logic operations. Until this century the spin of the electron was ignored in charge-based electronics. Charge of the electron is the information carrier in conventional electronics. However with emergence of the spintronics (spin electronics or spin-based electronics), electron's spin is also used as information carrier. Spintronics is a very wide research field with different aspects [8, 9].

As an example of spintronics, magnetoresistance effects' history dates back to 19th century. W. Thomson found the first experimental findings on the spin affected elec-

tron transport in 1857 which is the resistivity of bulk ferromagnetic metals increases when the current is in the same direction as the magnetic force and decreases when the current is at 90° to the magnetic force [10]. This phenomenon is called anisotropic magnetoresistance (AMR). In 1970 Tedrow and Meservey were the first ones to study spin polarized tunneling [11]. Five years later Julliere found that switching magnetic layers from the parallel to the antiparallel magnetization increased the resistance in some layered materials [12]. This is much stronger than AMR effect and is called tunneling magnetoresistance (TMR). Another well known magnetoresistance effect is the giant magnetoresistance (GMR) which was discovered in 1988 [13–15]. Similar to TMR setup, GMR devices consist two or more ferromagnets separated by a non-magnetic metal. While the underlying physics in TMR effect is governed by quantum mechanical tunneling, at GMR effect it is governed by diffusive transport. In both TMR and GMR, the resistance of ferromagnetic layers depends on the relative angle between the magnetizations in the ferromagnets. After the discovery of the GMR effect it was used to improve the sensitivity of read heads in hard drives which allowed decreasing the size of the magnetic bits and increased the data storage density of the hard disks dramatically. As a result, the discovery of the GMR effect has been awarded with the Nobel Prize in 2007. In the early experiments TMR was much smaller than GMR values. But with the support of recent years' theoretical studies [16, 17], TMR values exceeded the GMR values [18, 19].The most promising device of the TMR is magnetic random access memory (MRAM) and has recently become commercialized [19].

Another example for spintronics is spin Hall effect. The spin Hall effect is occurred as a result of spin-orbit interaction, and refers to the generation of a pure spin current at the lateral surfaces of an sample transverse to an applied electric field even in the absence of applied magnetic fields [20]. Early theoretical studies predicted an extrinsic spin Hall effect which is originating from asymmetries in scattering for up and down spins [21–24]. And more recently an intrinsic version of spin Hall effect is observed in semiconductors which is due to spin-orbit coupling even in the absence of impurities [25, 26]. In near future a spin current without any charge current may be obtained with spin Hall effect.

Using molecules as electronic devices is a promising new direction in the science and technology of mesoscopic systems [27, 28]. Experiments to today have studied a multitude of molecular devices in which molecules form basic components such as switches [29–31], diodes [32] and electronic mixers [33]. The latter includes molecules probed in a two-contact geometry using mechanically controlled break junctions [31, 34] or scanning

probes [35, 36] in addition to three-contact single molecule transistors made from carbon nanotubes [37] (CNT), C60 molecules [38] (Fullerenes), and conjugated molecules diluted in a less-conducting molecular layer [39]. And a very recent discovery [40] brought us one step closer to single atom transistor which is a device between two contacts where electrons hop on to and off from.

Integrating the molecular electronics with spintronics is very promising research area due to weak spin-orbit and hyperfine interactions in organic molecules, which leads to the possibility of preserving spin-coherence over times and distances much longer than in conventional metals or semiconductors [41]. A few recent experiments indicating e.g. a long spin-flip scattering length for CNTs [42], spin injection from strongly spin polarized materials into CNTs [43], and spin transport through organic molecules [44]. Also several theoretical studies have calculated spin-polarized transport in molecules [45, 46], including recent studies [41, 47] that combine density functional theory [48] and non-equilibrium Green function methods.

After the discovery of the carbon fullerenes [49], allotropes of carbon have become of great interest for research in material science. These days, a wide range of structures such as buckyballs, CNTs, or a combination thereof (carbon nanobuds) are well known. In principle, these structures consist of a single or several layers of graphite wrapped up in different configurations. Until it's experimentally observation [50] in 2004 the existence of a single layer of graphite, not wrapped up, was long thought to be thermodynamically unstable [51–54]. Single-layered graphite, graphene, has been the focus for intense research during the past few years. Graphene's low-energy physics is governed by the Dirac equation, and hence graphene exhibits many unique electronic properties, such as the odd-integer quantum Hall effect [55] that can be observed even at room temperature [56] and Klein tunneling [57]. More importantly graphene shows an exceptionally high mobility [58, 59] even at room-temperature [50, 55]. Thus, with graphene it might be possible to produce a room-temperature ballistic field-effect transistor, operating at much higher frequencies than conventional transistors. Also graphene is a promising candidate for spintronics with these unique electronic properties and very long spin relaxation time [60–62].

Recent years' advances in experimental techniques brought great challenges and new opportunities to the theory. The detailed configuration and conformation of molecules under the influence electrodes or the effects of electrode-molecule interactions will strongly affect the transport properties of the junctions. These elements could not be completely characterized so far. Theoretical numerical simulation is the most effective approach to

perform ideal experiments and design molecular devices with specific electronic properties.

Quantum theory has been the most appropriate theory to describe atomic-scale objects [63] and primary tool in the theoretical investigation of atoms, molecules and condensed matter. Atoms consist of nuclei and electrons. Both the dynamics of nuclei and electrons can be described by quantum theory. Moreover the physical properties of molecules, solids or more complicated systems can be investigated or predicted with quantum theory. Like Dirac proposed [64] eighty years ago, we have almost all rules to describe the world, but equations are too complex to solve analytically. Much effort has been devoted into the development of mathematical skills and numerical methods, such as the self-consistent field [65] (SCF) method, density functional theory (DFT) [48], quantum Monte Carlo methods [66], and so on. The equations are so complex due to the so many degrees of freedom so there is no exact analytic solution for almost all the systems encountered in practice except most simple systems such as Hydrogen atom. In this context the only practical approach is to calculate the properties approximately by employing various approximations to models.

In this thesis electronic, spintronics and transport properties of molecules and quasi one-dimensional systems are investigated by using state-of-the-art simulation methods based on electronic structure theory. One of the most promising tools of ab initio electronic structure method based on localized atomic orbitals is SIESTA [67, 68] In this thesis SIESTA simulation package was employed to compute electronic and magnetic properties of these systems.

At present, the most widely used simulation method in molecular electronics is non-equilibrium Green's function (NEGF) technique combined with DFT. Several simulation schemes have been implemented [69–73] and contributed a lot to the advance of this area. Also in this thesis, TRANSIESTA [67, 68, 74] and SMEAGOL [41]tool was employed to calculate transport properties of these systems.

CHAPTER 2

MATERIAL

2.1. Nanowires and Molecular Structures

Miniaturization of integrated circuits is steadily approaching a new state: atomic size devices connected by atomic wires. To build these state of the art devices, manufacturers are focusing their research on the self-assembly of surface nanostructures and nanowires.

Nanowires have many novel properties which can be only seen in one dimensional systems. This behavior is due to electrons in one dimensional systems are confined laterally and thus occupy energy bands that are different from the energy bands found in bulk systems. Nanowires' intrinsic one dimensional nature makes them ideal for studying dimensionality effects on e.g. magnetic and electronic properties [75–81]. Molecular nanowires are composed of repeating organic, inorganic or ,as in one of our cases, organometallic molecule's unit cells. Examples of nanowires and their possible applications can be seen in Figure 2.1.

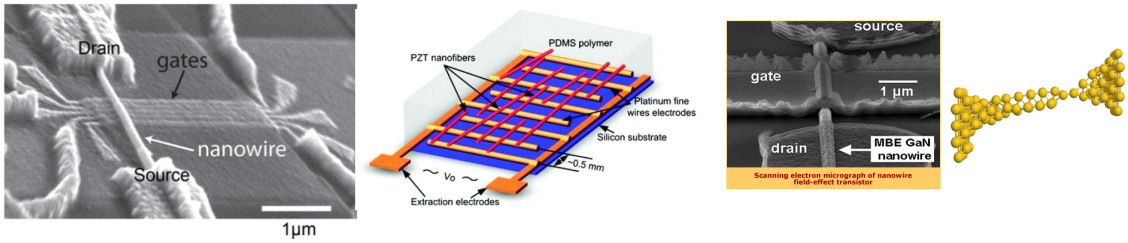

Figure 2.1. Left to right; images of nanowire device with gate electrodes (Source: [82]), a piezoelectric nanogenerator based on PZT nanofiber (Source: [83]), a nanowire field-effect transistor (Source: [84]), and a stretched gold nanowire (Source: [85]), respectively.

The electrical and mechanical properties of a piece of any metal are not different for its any macroscopic size. However, as soon as its size decreases to the nano scale, all common knowledge becomes unreliable. One example to the that is Ohm's Law, which is that the resistance of a conductor scales proportional to its length, does not hold any more due to the atomic sizes become much larger than the electron's mean free path (distance of

an electron travels between two scattering events). The resistance becomes independent of its length due to the electrons traverse an nano-conductor ballistically.

The electrical conductance through an one atom thick nanowire is quantized as $G = 2\,e^2/h$, where e is the charge on an electron and h is Planck's constant. So the conductance of nanowires is only expected to be multiple of the this constant.

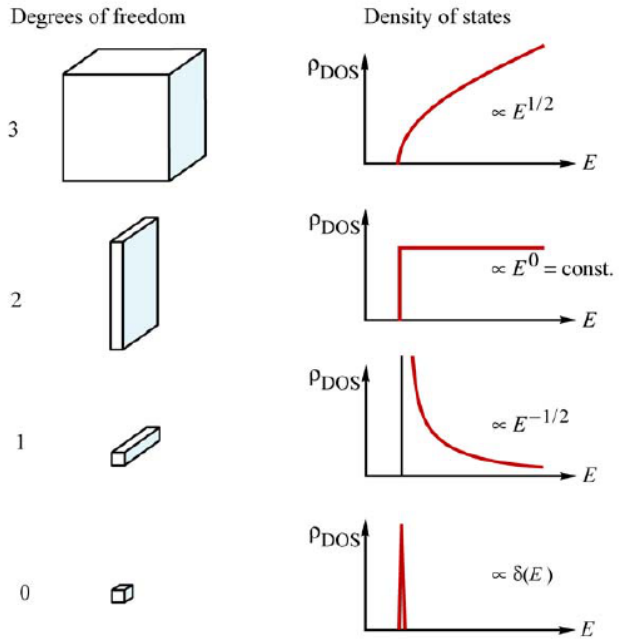

Figure 2.2. Density of States Diagrams for 0, 1, 2, 3 Dimensions. (Source: [86])

The energy dispersion relations and density of states plots of the free electron gas from 0 to 3 dimensions are represented In Figure 2.2. The more specific form of density of states in one dimension is:

$$D_1(\varepsilon) = \frac{2}{\pi}\,\frac{1}{|d\varepsilon_k/dk|} \tag{2.1}$$

In one dimension energy diverges at the beginning or end of a range of allowed energies. These divergences are called van Hove singularities. This behavior of energy divergences of at a minimum or maximum is characteristic for one dimensional structures which they will be encountered at the structures studied in this thesis.

As a part of the a nanowire, zero dimensional molecules are very important for molecular electronics where explained in detail at chapter 1. Similarly in zero dimension

energy dispersion relation is

$$D_0(\varepsilon) = 2\, n_i \sum_k \delta(\varepsilon - \varepsilon_k) \tag{2.2}$$

Since the energy levels of system, that are quantized in all there dimensions discrete, the DOS is a couple of delta functions with peaks at discrete energies. This DOS plot is characteristic for zero dimensional systems. In this thesis particularly nanowires' molecular part's transport properties will be investigated through by connecting them with different leads and applying voltage.

2.2. Graphene

It has been more than sixty years since the first theoretical study of graphene was performed [87]. However, graphene could not draw enough attention till 2004 which explained in detail at chapter 1. After its isolation as single layer in 2004 [50], graphene has become a material of great interest for research in material science due to its peculiar electronic properties.

2.2.1. Structural and Electronic Properties

Graphene is a single layer of graphite with a honeycomb two-dimensional lattice (see Figure 2.3). The two lattice vectors can be expressed as

$$\mathbf{a_1} = a(\frac{3}{2}, \frac{\sqrt{3}}{2}), \quad \mathbf{a_2} = a(\frac{3}{2}, -\frac{\sqrt{3}}{2}) \tag{2.3}$$

where a$= 1.42$ Å is the carbon-carbon bond length. The reciprocal lattice vectors can be calculated as following

$$\mathbf{b_1} = \frac{2\pi}{a}(\frac{1}{3}, \frac{\sqrt{3}}{3}), \quad \mathbf{b_2} = \frac{2\pi}{a}(\frac{1}{3}, -\frac{\sqrt{3}}{3}) \tag{2.4}$$

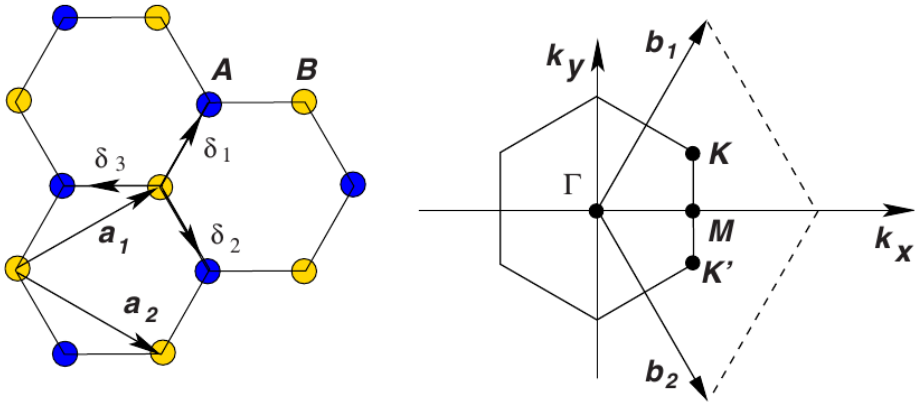

Figure 2.3. Honeycomb lattice and its Brillouin zone. $\mathbf{a}_1$ and $\mathbf{a}_2$ are the lattice unit vectors and δ_i, $i = 1, 2, 3$ are the nearest-neighbor vectors. (Source: [88])

which the first Brillouin zone (BZ) can be constructed by using a Wigner-Seitz cell method [89]. In Figure 2.4 the energy band diagram along high-symmetry directions in the first BZ is presented. It can be seen that the honeycomb lattice symmetry lead to a peculiar band structure, where the conduction and valance band meet each other at six points and coincide with the corners of BZ (**K** and **K'**). Therefore graphene is a semimetal (zero band gap semiconductor). These points are named as Dirac points due to energy dispersion relationship near this points. Their positions in momentum space are given by

$$\mathbf{K} = \frac{2\pi}{a}(\frac{1}{3}, \frac{1}{3\sqrt{3}}), \quad \mathbf{K}' = \frac{2\pi}{a}(\frac{1}{3}, -\frac{1}{3\sqrt{3}}). \tag{2.5}$$

And nearest-neighbor vectors are

$$\delta_1 = \frac{a}{2}(1, \sqrt{3}), \quad \delta_2 = \frac{a}{2}(1, -\sqrt{3}), \quad \delta_3 = -a(1, 0). \tag{2.6}$$

Linear energy dispersion relation near Fermi level is calculated by Wallace at 1947 [87]

$$E_{\pm}(\mathbf{q}) \approx \pm v_F|\mathbf{q}| + O[(q/K)^2]. \tag{2.7}$$

This dispersion leads to Fermi velocities of charge carriers v_F reaching the value 1/300 of the speed of light c. In this thesis graphene defects and ad-atom absorption on these defect sites will be studied.

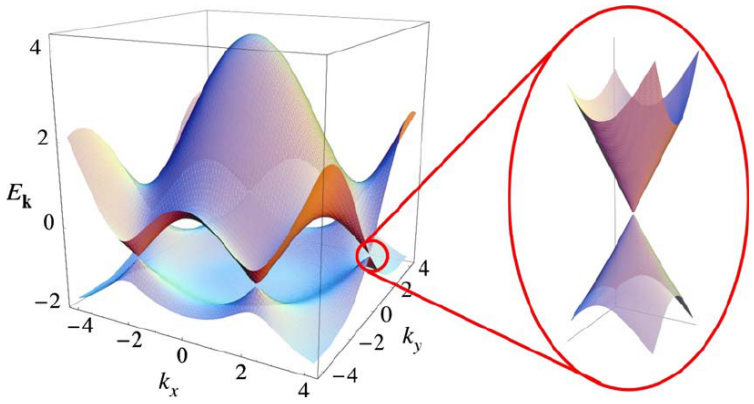

Figure 2.4. Energy dispersion in the honeycomb lattice. Energy is in units of t where $t = 2.7$ eV. (Source: [88])

2.2.2. Graphene Nano Ribbons

Recent experimental studies allow the preparation of graphene nanoribbon (GNR), which is a graphene layer terminated in one direction with a specific width[90, 91]. And recently, sub 10 nm GNRs with smooth edges were obtained and demonstrated to be semiconductor. In Figure 2.5 we see a honeycomb lattice having zigzag edges along x direction and armchair edges along the y direction. Geometrical termination of graphene

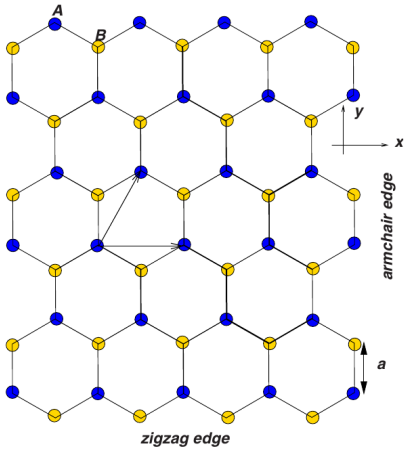

Figure 2.5. A piece of a honeycomb lattice displaying both zigzag and armchair edges. (Source: [88])

lead to two edge geometries, namely, zigzag and armchair with largely varying electronic properties. Studies have shown that zigzag edge GNRs (ZGNRs) are semiconductors with two localized electronic edge states[92–96]. These two states are ferromagnetically ordered and they antiferromagnetically coupled to each other [97]. In this thesis ZGNRs'

will be studied rather than armchair GNRs (AGNRs) due to ZGNRs novel magnetic and electronic properties.

CHAPTER 3

CALCULATION METHODS AND APPROXIMATIONS

3.1. Quantum Theory and Electronic Structure

Theory of electrons in matter has been one of the great challenges of theoretical physics after the discovery of the electron in 1896-1897. The understanding of materials and phenomena rests upon understanding electronic structure. Theory of electrons in matter rely on: developing theoretical approaches and computational methods that can accurately treat the interacting system of many electrons and nuclei which in molecules and condensed matter.

Most of the many-body systems e.g. condensed matter systems where the total number of electrons is nearly Avogadro constant ($N_A \sim 6.02 \times 10^{23}$). This massive degrees of freedom requires a statistical physics point of view to overcome electronic structure problems. In 1925, Pauli proposed periodic table of elements in terms of electrons obeying the exclusion principle that no two electrons can be in the same quantum state [98]. Nearly one year later Fermi [99] generalized the exclusion principle to the general formula for the statistics of non-interacting particles and linked the correspondence to the analogous formula for Bose-Einstein statistics [100, 101] (see Equation 3.1).

$$f_i = \frac{1}{e^{\beta(\epsilon_i - \mu} \pm 1}, \tag{3.1}$$

where, f_i is the occupation number of electrons on the i-th energy level, $\beta = 1/k_B T$, relates to Boltzmann constant k_B and temperature T, ϵ_i is the i-th eigenenergy, μ is the chemical potential of system, plus sign is for Fermi-Dirac and the minus sign is for Bose-Einstein statistics. Also in 1926 by Heisenberg [102] as first and by Dirac [103] in 1926 independently discussed the general principle that when two particles are exchanged the wavefunction for identical particles must be either symmetric or antisymmetric.

Simulating physical properties of systems is just solving many-body Schrödinger equation of the systems by quantum mechanics. The Hamiltonian of a typical many-body

system can be written as

$$\mathcal{H} = \mathcal{T} + \mathcal{T}_n + \mathcal{V}_{int} + \mathcal{V}_{nn} + \mathcal{V}_{ext}. \tag{3.2}$$

The terms in Hamiltonian are:

$$\mathcal{T} = -\frac{\hbar^2}{2m_e} \sum_i \nabla_i^2 \tag{3.3}$$

where $\mathcal{T}$ is the electron kinetic energy;

$$\mathcal{T}_n = -\sum_I \frac{\hbar^2}{2M_I} \nabla_I^2 \tag{3.4}$$

where $\mathcal{T}_n$ is the nuclei kinetic energy;

$$\mathcal{V}_{int} = \frac{1}{2} \sum_{i \neq j} \frac{e^2}{|\mathbf{r_i} - \mathbf{r_j}|} \tag{3.5}$$

where $\mathcal{V}_{int}$ is the electron-electron repulsion term;

$$\mathcal{V}_{nn} = \frac{1}{2} \sum_{I \neq J} \frac{Z_I Z_J e^2}{|\mathbf{R_I} - \mathbf{R_J}|} \tag{3.6}$$

where $\mathcal{V}_{nn}$ is the nuclei-nuclei repulsion term;

$$\mathcal{V}_{ext} = -\sum_{i,I} \frac{Z_I e^2}{|\mathbf{r_i} - \mathbf{R_I}|} \tag{3.7}$$

and where $\mathcal{V}_{ext}$ is the attractive interaction term between the electrons and the nuclei described as an external potential for the electrons. And in general m_e and $\mathbf{r_i}$ are the electron mass and positions, M_I are the masses of the nuclei, R_I the corresponding positions, and Z_I is the nuclear charge.

Complexity of the problem creates too many degrees of freedom in problem and makes an “ab-initio” manner is impossible. Thus various approximations is necessary to reduce the calculation into a acceptable level.

3.2. Approximations

3.2.1. Born-Oppenheimer

Born-Oppenheimer (adiabatic) approximation is basicly setting the mass of nuclei to infinity. Since mass of nuclei is immensely larger than mass of electron. Thus when dealing with electron-nuclei many body systems, the kinetic energy of the can be ignored. Adiabatic approximation reduces the number of degrees of freedom of the system so all the contribution from nuclei interactions (V_{nn}) is now nothing but a constant.

3.2.2. Pseudopotential

The electrons fill the lowest energy states up to a Fermi energy and leaving empty states above this energy for zero temperature and magnetic field. For non-zero but low magnetic field and temperature, only the electronic states near Fermi energy are able to effect physical properties of solids. In this context pseudopotential approximation is introduced.The basic idea behind the pseudopotential is replacing the strong Coulomb potential of the nucleus and the effects of the core electrons by an effective ionic potential acting on the valance electrons. Figure 3.1 illustrates the all-electronic wavefunctions and generated pseudo wavefunction and corresponding potentials. Pseudopotentials generated by atomic calculations are defined “ab initio” since they are not fitted to experiment. Thus their accuracy and transferability requires the concept of several conditions;

1. The pseudo wavefunctions and atomic wavefunctions must produce same core charge.
2. The pseudo-electron eigenvalues and the valance eigenvalues must be same.
3. The pseudo wavefunctions, and their first and second derivatives must be continuous at the core radius and non-oscillatory inside the core radius.
4. The pseudo wavefunctions and atomic wavefunctions must agree beyond the core radius.

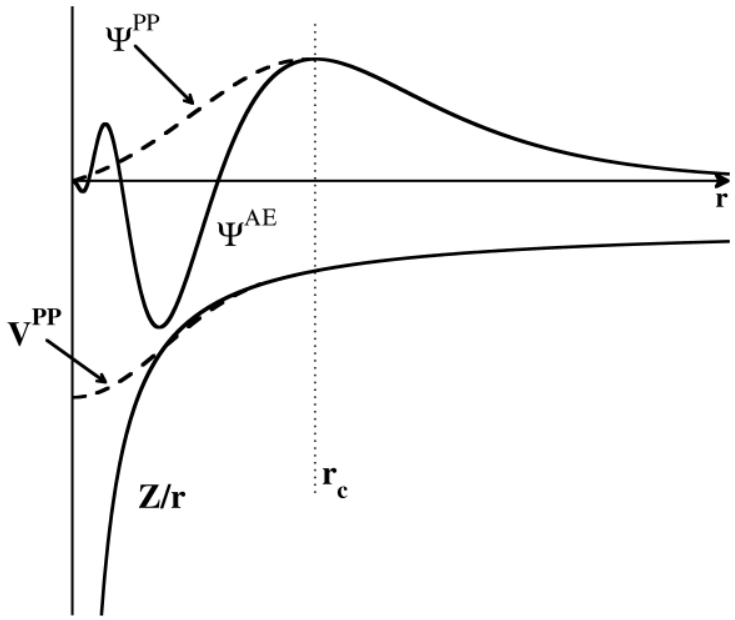

Figure 3.1. Pseudopotentials are generated in such a way that the pseudo wavefunction contains no nodes inside the core region $r < r_c$ and becomes the exact all-electron wavefunction for $r > r_c$. (Source: [104])

3.2.3. Non-relativistic

Objects with massive body or with speed comparable with that of light could only be described exactly in the relativistic framework. In "ab-initio" calculations, small mass of electrons and in most of the atoms a non-relativistic approach should be enough to investigate problem. But, when working with heavy atoms the relativistic effects may not be ignored anymore due to the high speed of core electrons in heavy atoms.

There are several approaches to integrate relativistic effects into "ab-initio" calculations. One of the most important method is using relativistic pseudopotentials. In this method relativistic Dirac equation is used for atomic calculations during the building of pseudopotentials. Thus these relativistic pseudopotentials may be used to construct Hamiltonian. In this thesis the relativistic pseudoptential approach will be used to carry out calculations in the relativistic framework.

3.3. Density Functional Theory

The many-body Schrödinger equation can in principle be solved by expanding the wavefunction in a basis of Slater determinants. For N-electron system, the single Slater

determinant can be written as:

$$\Psi = \frac{1}{N!^{1/2}} \begin{vmatrix} \phi_1(\mathbf{r_1}, \sigma_1) & \phi_1(\mathbf{r_2}, \sigma_2) & \phi_1(\mathbf{r_3}, \sigma_3) & \cdots \\ \phi_2(\mathbf{r_1}, \sigma_1) & \phi_2(\mathbf{r_2}, \sigma_2) & \phi_2(\mathbf{r_3}, \sigma_3) & \cdots \\ \phi_3(\mathbf{r_1}, \sigma_1) & \phi_3(\mathbf{r_2}, \sigma_2) & \phi_3(\mathbf{r_3}, \sigma_3) & \cdots \\ \vdots & \vdots & \vdots & \ddots \end{vmatrix} \tag{3.8}$$

where $\phi_i(\mathbf{r}_j, \sigma_j)$ is the single-electron spin orbital, and it is the product of position $\psi_i(\mathbf{r}_i)$ and spin $\alpha_i(\sigma_i)$ component. Thus this converts calculation to the diagonalizing a matrix. But this can only be done for very small systems since the dimension of the Slater basis grows with the number *N* of electrons as $N!$. Before the advent of DFT, the standard approach has been to approximate the many-body wave function by a single Slater determinant that minimizes the total energy. This is the Hartree-Fock approximation. However, Hartree-Fock approximation gives a very crude description of the electronic structure since correlations between electrons are neglected but instead electrons are described as independent of each other and interacting via an effective mean field.

As an alternative approach density functional theory states in general that any property of a many interacting system can described in terms of the ground state density $n_0(\mathbf{r})$ where $n_0(\mathbf{r})$ is a scalar function of position. Thus in principle, a functional of the ground state density determines all the information for the ground state and excited states.

3.3.1. Thomas-Fermi-Dirac Approximation

Density functional theory proposed first time in 1927 by Thomas [105] and Fermi [106], where they expressed the kinetic energy in terms of electron density. Both Thomas and Fermi neglected exchange and correlation among the electrons. This was extended by Dirac [107] three years later who formulated the local approximation for exchange. This formulation for exchange is still in use today. In Thomas-Fermi-Dirac approximation, the

energy functional is expressed as

$$E_{TF}[n] = C_1 \int d^3r\, n(\mathbf{r})^{5/3} + \int d^3r\, V_{ext}(\mathbf{r})\, n(\mathbf{r}) \\ + C_2 \int d^3r\, n(\mathbf{r})^{4/3} + \frac{1}{2} \int d^3r\, d^3r'\, \frac{n(\mathbf{r})n(\mathbf{r}')}{|\mathbf{r} - \mathbf{r}'|} \tag{3.9}$$

where the first term is the local approximation to the kinetic energy, third term is the local approximation of exchange energy, and last term is the classical electrostatic Hartree energy. Despite this approximation lead to one equation for the density which it is simpler than the full many-body Schrödinger equation that involves $3N$ degrees of freedom for N electrons, it lack in detailed physical and chemical information. Thus this restricts its application in actual calculations.

3.3.2. Hohenberg-Kohn Theorems

In 1964 Hohenbern and Kohn proposed two theorems to formulate density functional theory as an exact theory of many-body systems [48]. These theorems are commonly accepted as the onset of modern DFT. The two theorems are

Theorem I : *For any system of N-interacting electrons, any of its physical properties are completely determined by the ground state electron density n(**r**).*

Theorem II : *The global minimum of energy functional is the ground state energy, and the corresponding electron density is the ground state density.*

The Hamiltonian of many-body system can be written with the approximations which they are explained above

$$\mathcal{H} = -\frac{\hbar^2}{2m_e} \sum_i \nabla_i^2 + \sum_i \mathcal{V}_{ext}(\mathbf{r}_i) + \frac{1}{2} \sum_{i \neq j} \frac{e^2}{|\mathbf{r}_i - \mathbf{r}_j|} \tag{3.10}$$

And the energy functional can be expressed as

$$\begin{aligned} E_{HK}[n] &= T[n] + E_{int}[n] + \int d\mathbf{r}\, V_{ext}(\mathbf{r})\, n(\mathbf{r}) + E_{II} \\ &= F_{HK}[n] + \int d\mathbf{r}\, V_{ext}(\mathbf{r})\, n(\mathbf{r}) + E_{II} \end{aligned} \tag{3.11}$$

where E_{II} is nucleus-nucleus interaction, $F_{HK}[n]$ is system internal energy, including electron kinetic, potential and interaction energy. So if we know $F_{HK}[n]$ then we can determine the electron density of the ground state by simply minimizing the energy functional.

3.3.3. The Kohn-Sham Equations

Since there has been made no approximations so far, DFT is in principle an exact theory. However, the drawback is that the exact energy functional is not known so one needs to adopt schemes for obtaining an expression for it that can later be used in the computations. In 1965, Kohn and Sham [108] proposed that to replace the original many-body problem by an auxiliary independent-particle problem with all the interactions between electrons are classified into a exchange-correlation term. The auxiliary hamiltonian of the auxiliary independent-particle system is (using Hartree atomic units $\hbar = m_e = e = 4\pi/\epsilon_0 = 1$)

$$\mathcal{H}^{\sigma}_{aux} = -\frac{1}{2}\nabla^2 + \mathcal{V}^{\sigma}(\mathbf{r}) \tag{3.12}$$

where $\mathcal{V}^{\sigma}(\mathbf{r})$ is a potential acting on an electron of spin σ at point $\mathbf{r}$. And the electron density

$$n(\mathbf{r}) = \sum_{\sigma} n(\mathbf{r}, \sigma) = \sum_{\sigma} \sum_{i=1}^{N^{\sigma}} |\psi_i^{\sigma}(\mathbf{r})| \tag{3.13}$$

where ψ_i^σ is the i-th single particle orbital with spin component σ. Thus the independent-particle kinetic energy T_s is given by

$$T_s = -\frac{1}{2}\sum_\sigma \sum_{i=1}^{N^\sigma} \langle \psi_i^\sigma | \nabla^2 | \psi_i^\sigma \rangle = \frac{1}{2}\sum_\sigma \sum_{i=1}^{N^\sigma} |\nabla \psi_i^\sigma|^2, \tag{3.14}$$

and the classical Coulomb interaction term can be defined as the interaction between electron density with itself

$$E_{Hartree}[n] = \frac{1}{2}\int d\mathbf{r}\, d\mathbf{r}' \frac{n(\mathbf{r})n(\mathbf{r})}{|\mathbf{r}-\mathbf{r}'|} \tag{3.15}$$

Hohenberg-Kohn expression for the ground state energy functional is rewritten in the Kohn-Sham approach as

$$E_{KS} = T_s[n] + \int d\mathbf{r}\, V_{ext}(\mathbf{r})n(\mathbf{r}) + E_{Hartree}[n] + E_{II} + E_{xc}[n] \tag{3.16}$$

All many-body effects of exchange and correlation are included into the exchange correlation energy $E_{xc}[n]$. Khon-Sham independent-particle problem can be solved by minimization with respect to density $n(\mathbf{r}, \sigma)$. All terms except the independent-particle kinetic energy T_s are considered to be functionals of the density. Thus with using the fact that T_s is explicitly expressed as a functional of the orbitals, one can derive the variational equation

$$\frac{\delta E_{KS}}{\delta \psi_i^{\sigma *}(\mathbf{r})} = \frac{\delta T_s}{\delta \psi_i^{\sigma *}(\mathbf{r})} + \left[\frac{\delta E_{ext}}{\delta n(\mathbf{r},\sigma)} + \frac{\delta E_{Hartree}}{\delta n(\mathbf{r},\sigma)} + \frac{\delta E_{xc}}{\delta n(\mathbf{r},\sigma)}\right]\frac{\delta n(\mathbf{r},\sigma)}{\delta \psi_i^{\sigma *}(\mathbf{r})} = 0, \tag{3.17}$$

also the orthonormalization condition requires

$$\langle \delta\psi_i^\sigma | \delta\psi_j^{\sigma'} \rangle = \delta_{i,j}\delta_{\sigma,\sigma'}. \tag{3.18}$$

Using equations 3.13 and 3.14 in 3.17 gives

$$\begin{aligned} \frac{\delta T_s}{\delta \psi_i^{\sigma *}(\mathbf{r})} &= -\frac{1}{2}\nabla^2 \psi_i^{\sigma}(\mathbf{r}) \\ \frac{\delta n^{\sigma}(\mathbf{r})}{\delta \psi_i^{\sigma *}(\mathbf{r})} &= \psi_i^{\sigma}(\mathbf{r}) \end{aligned} \tag{3.19}$$

and using the Lagrange multiplier method to handle constraints leads to the Khon-Sham Schödinger-like equations:

$$\left(\mathcal{H}_{KS}^{\sigma} - \epsilon_i^{\sigma}\right) \psi_i^{\sigma}(\mathbf{r}) = 0 \tag{3.20}$$

where ϵ_i^{σ} are Khon-Sham eigenenergies. And $\mathcal{H}_{KS}^{\sigma}$ is the effective hamiltonian

$$\mathcal{H}_{KS}^{\sigma}(\mathbf{r}) = -\frac{1}{2}\nabla^2 + V_{KS}^{\sigma}(\mathbf{r}) \tag{3.21}$$

where V_{KS}^{σ} is Kohn-Sham potential and it is defined as

$$V_{KS}^{\sigma}(\mathbf{r}) = V_{ext}(\mathbf{r}) + \frac{\delta E_{Hartree}}{\delta n((\mathbf{r}), \sigma)} + \frac{\delta E_{xc}}{\delta n((\mathbf{r}), \sigma)}$$

$$V_{KS}^{\sigma}(\mathbf{r}) = V_{ext}(\mathbf{r}) + V_{Hartree}(\mathbf{r}) + V_{xc}^{\sigma}(\mathbf{r}). \tag{3.22}$$

Equations (3.20)-(3.22) are the Khon-Sham equations. These equations must be solved with in a self-consistently way. Also the Kohn-Sham equations are independent of the any approximation to the exchange-correlation energy functional $E_{xc}[n]$.

If we summarize the Kohn-Sham procedure:

I. Initial guess for density $n^{\uparrow}(\mathbf{r}), n^{\downarrow}(\mathbf{r})$

II. Calculate Kohn-Sham potential $V_{KS}^{\sigma}(\mathbf{r})$

III. Solve Khon-Sham equations, eq. (3.20) and (3.21)

IV. Calculate electron density $n^{\uparrow}(\mathbf{r}), n^{\downarrow}(\mathbf{r})$ from eq. (3.13)

V. Repeat from step II until $n^{\uparrow}(\mathbf{r}), n^{\downarrow}(\mathbf{r})$ is converged

VI. If self-consistency is archived, then output quantities e.g. energy, Hellmann-Feynman forces [109, 110], stresses [111, 112], eigenvalues can be calculated.

Once Hellmann-Feynmann forces and stresses are calculated the system can be relaxed geometrically [113] and find local minimum around given initial coordinates.

The Khon-Sham orbitals are usually described as linear combinations of a set of functions, e.g. basis set. In principle basis set must be infinite to solve problem. But in practice it is impossible to implement these large basis sets. Thus a cutoff value is used to truncate the number of dimensions. Some examples of basis sets to be used in Khom-Sham equations :

1. Slater type orbitals[114]
2. Gaussian type orbitals[115]
3. Plane waves[116]
4. Wannier functions[117]
5. Wavelets[118]
6. Linear combinations of atomic orbitals (LCAO) [119]

In this thesis LCAO basis set is used for the Khon-Sham orbitals.

3.3.4. Exchange-Correlation Functionals

All the unknown variables of the problem are now collected in the exchange-correlation term, which must be approximated. The explicit separation of kinetic and Hartree energy term implies that exchange-correlation functional would be localized [116]. The exact expression of the exchange-correlation potentials should be very complex. However there are some clues from its various boundary conditions.

3.3.4.1. Local (Spin) Density Approximation, L(S)DA

LDA is a simple approximation assuming that the electron density is only slightly modulated by the potential of the ion cores. Thus the exchange-correlation functional is

given by [108, 120]

$$E_{xc}^{LDA}[n^{\uparrow}, n^{\downarrow}] = \int d^3r\, n(\mathbf{r})\, \varepsilon_{xc}(n^{\uparrow}(\mathbf{r}), n^{\downarrow}(\mathbf{r})), \tag{3.23}$$

where $\varepsilon_{xc}(n^{\uparrow}(\mathbf{r}), n^{\downarrow}(\mathbf{r}))$ is the exchange-correlation energy per particle for a homogeneous electron gas with density $(n(\mathbf{r}))$ and can be split into two as

$$\varepsilon_{xc}(n^{\uparrow}(\mathbf{r}), n^{\downarrow}(\mathbf{r})) = \varepsilon_{x}(n^{\uparrow}(\mathbf{r}), n^{\downarrow}(\mathbf{r})) + \varepsilon_{c}(n^{\uparrow}(\mathbf{r}), n^{\downarrow}(\mathbf{r})) \tag{3.24}$$

The exchange part for the homogeneous electron gas can be calculated with Hartree-Fock method as

$$\varepsilon_{x}(n^{\uparrow}(\mathbf{r}), n^{\downarrow}(\mathbf{r})) = -\frac{1}{2^{2/3}}\frac{3}{8}e^2\left(\frac{3}{\pi}\right)^{1/3}(n^{\uparrow}(\mathbf{r}))^{1/3} - \frac{1}{2^{2/3}}\frac{3}{8}e^2\left(\frac{3}{\pi}\right)^{1/3}(n^{\downarrow}(\mathbf{r}))^{1/3} \tag{3.25}$$

The calculation of the correlation term $\varepsilon_{c}(n^{\uparrow}(\mathbf{r}), n^{\downarrow}(\mathbf{r}))$ is more difficult to calculate. Using Monte Carlo method [121] it may be computed accurately. The LDA has been quite successful in describing ground state properties of materials with small variations in the electronic density e.g. metallic systems. When there are strong gradients the LDA is not an effective approximation. Also, the band gaps in semiconductors and insulators are usually underestimated by % 40.

3.3.4.2. Generalized Gradient Approximation, GGA

A logical step to improve LDA is using a XC functional which contains electron density with its gradient as [122]:

$$E_{xc}^{GGA}[n^{\uparrow}, n^{\downarrow}] = \int d^3r\, n(\mathbf{r})\, \varepsilon_{xc}(n^{\uparrow}(\mathbf{r}), n^{\downarrow}(\mathbf{r}), \nabla n^{\uparrow}(\mathbf{r}), \nabla n^{\downarrow}(\mathbf{r})). \tag{3.26}$$

GGA improves the description of transition metals considerably. GGA greatly increased the application areas of DFT. There are many GGA functionals e.g. Becke88 [123], PW91 [124], PBE [125]. In this thesis all of the calculations are carried out with GGA and tested

also with LDA.

3.3.4.3. Hybrid Functionals

The LDA and GGA method has been failing to describe electronic states of the d- and f-states of transition metals, and the orbitals of molecules due to artificial error for localized electron states. Thus an approach to fix the error from artificial self-interaction is the mixing Hartre-Fock exchange with GGA or LDA functional. A hybrid functional is made of two parts. The first part is exact exchange functional from Hartree-Fock theory and the second part is exchange-correlation from some other theory such as LSDA, GGA. The exact amount of Hartree-Fock exchange needs to be reintroduced in order to give a sufficient correction of the self-interaction error in the LSDA or GGA functional and it is unfortunately unknown. Thus it needs to be fitted to experiments [126]. DFT using hybrid functionals does not really represent an "ab-initio" method. However, hybrid functionals has been shown to improve the predictive power of DFT for a number of molecular properties such as atomisation energies, bond lengths and vibration frequencies [127].

3.3.4.4. LDA+U

Another approach to fix error from artificial self-interaction is introducing a Hubbard U parameter representing the screened electron-electron interaction in the d-orbitals of the transition metals and the f-orbitals of the rare earth metals. This U parameter is added to the LDA and treated in the Hartree-Fock approximation. However finding a suitable U parameter is done by extracting from a previous calculation or fitting to experiments. LDA+U method gives better results for strongly correlated materials than than the LDA method.

3.3.4.5. Exact Exchange Functionals

Deriving a local Kohn-Sham potential from the non-local exact exchange energy of the Hartree-Fock approximation is yet another way to treat the self-interaction error. The Exact Exchange potential is local in contrast to the Hybrid functional approach where the Hartree-Fock Exchange potential is inherently non-local. Cancellation of the exact ex-

change energy of the Hartree-Fock approximation with the self-interaction of the Hartree-term makes the The Exact Exchange method as self-interaction free. Thus a good approximation of the correlation energy (GGA or LDA) is combined with the Exact Exchange method gives an excellent description of the electron density. Also, unlike the Hybrid functional or LDA+U method, the Exact Exchange method does not need any empirical parameters. But as a drawback, the computational cost for the calculation of the Exact Exchange functional is very high compared to other methods [128–130].

3.4. Ballistic Quantum Conductance

Electron transport phenomena in low-dimensional system can be divided into two general parts. First one is diffusive transport which occurs when when the nanowire's length is much greater than the charge carrier mean free path, carriers scatter due to numerous events when they travel along the wire. On the other hand when the electrons travels across the nanowire without any scattering, the ballistic transport occurs. Therefore the contacts between the nanowire and the external circuit mainly effects the conduction. Ballistic transport is generally obtained with very short nanowires where the electron mean free path is much longer than the wire length. These short nanowires or molecules are non-equilibrium, non-periodic, and infinite with open boundary conditions.

The traditional quantum physics approaches can not deal with these systems properly since they take into account electron correlations in stationary systems. The non-equilibrium Green's function (NEGF) method can deal with these systems properly due to its general nature. NEGF's general useful properties are:

1. NEGF is function of two space-time coordinates. The time-dependent expectation values of currents, densities, electron addition and removal energies, and the total energy of the system can be calculated with NEGF method.

2. NEGF method reduces to the EGF in the absence of external fields.

3. NEGF can be applied to extended and finite systems.

4. NEGF can handle strong external fields without perturbatively. The electron-electron interactions are taken into account.

3.4.1. System and Model

A typical model for the a molecule or short nanowire is confined by two leads can be seen in Figure 3.2. Both electrodes are semi-infinite and continues periodically to both

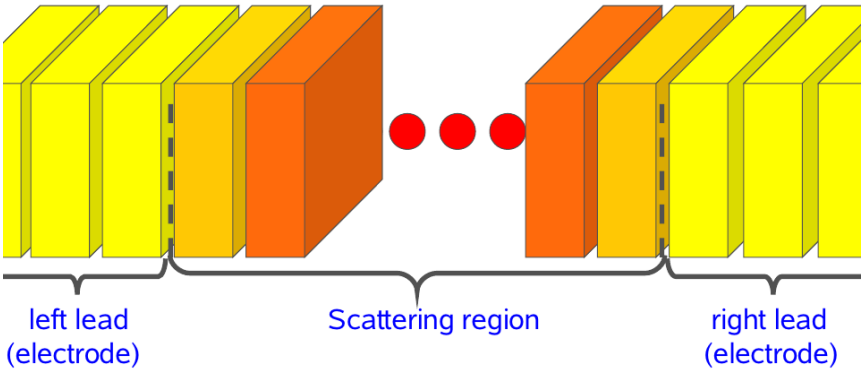

Figure 3.2. Model for the electron transport for the molecules or short nanowires. (Source: [131])

sides. It is commonly the scattering region is constructed with molecule or short nanowire and sufficient layers of the electrodes so interactions between electrodes are avoided. In this context, all the system has three parts, the scattering region is a finite system, and the leads are semi-infinite and periodic structures. The total Hamiltonian of the system include contributions from both scattering zone and leads;

$$\mathcal{H} = \begin{pmatrix} \mathbf{H}_{LL} & \mathbf{H}_{LC} & 0 \\ \mathbf{H}_{LC}^{\dagger} & \mathbf{H}_{CC} & \mathbf{H}_{CR} \\ 0 & \mathbf{H}_{CR}^{\dagger} & \mathbf{H}_{RR} \end{pmatrix} \tag{3.27}$$

And constructing the Green's function equation with the $\mathcal{H}$ yields;

$$\begin{pmatrix} E\mathbf{S}_{LL} - \mathbf{H}_{LL} & E\mathbf{S}_{LC} - \mathbf{H}_{LC} & 0 \\ (E\mathbf{S}_{LC} - \mathbf{H}_{LC})^{\dagger} & E\mathbf{S}_{CC} - \mathbf{H}_{CC} & E\mathbf{S}_{CR} - \mathbf{H}_{CR} \\ 0 & (E\mathbf{S}_{CR} - \mathbf{H}_{CR})^{\dagger} & E\mathbf{S}_{RR} - \mathbf{H}_{RR} \end{pmatrix} \begin{pmatrix} \mathbf{G}_{LL} & \mathbf{G}_{LC} & \mathbf{G}_{LR} \\ \mathbf{G}_{CL} & \mathbf{G}_{CC} & \mathbf{G}_{CR} \\ \mathbf{G}_{RL} & \mathbf{G}_{RC} & \mathbf{G}_{RR} \end{pmatrix} = \begin{pmatrix} \mathbf{I}_{LL} & 0 & 0 \\ 0 & \mathbf{I}_{CC} & 0 \\ 0 & 0 & \mathbf{I}_{RR} \end{pmatrix} \tag{3.28}$$

where $\mathbf{S}$ and $\mathbf{I}$ overlap and unitary matrices, respectively. One needs to solve the above equation to obtain Green's function of the system. Matrix multiplication yields;

$$(E\mathbf{S}_{LL} - \mathbf{H}_{LL})\mathbf{G}_{LL} + (E\mathbf{S}_{LC} - \mathbf{H}_{LC})\mathbf{G}_{CL} = \mathbf{I}_{LL} \tag{3.29}$$

$$(E\mathbf{S}_{LL} - \mathbf{H}_{LL})\mathbf{G}_{LC} + (E\mathbf{S}_{LC} - \mathbf{H}_{LC})\mathbf{G}_{CC} = \mathbf{0} \tag{3.30}$$

$$(E\mathbf{S}_{LL} - \mathbf{H}_{LL})\mathbf{G}_{LR} + (E\mathbf{S}_{LC} - \mathbf{H}_{LC})\mathbf{G}_{CR} = \mathbf{0} \tag{3.31}$$

$$(E\mathbf{S}_{LC} - \mathbf{H}_{LC})^{\dagger}\,\mathbf{G}_{LL} + (E\mathbf{S}_{CC} - \mathbf{H}_{CC})\mathbf{G}_{CL} + (E\mathbf{S}_{CR} - \mathbf{H}_{CR})\mathbf{G}_{RL} = \mathbf{0} \tag{3.32}$$

$$(E\mathbf{S}_{LC} - \mathbf{H}_{LC})^{\dagger}\,\mathbf{G}_{LC} + (E\mathbf{S}_{CC} - \mathbf{H}_{CC})\mathbf{G}_{CC} + (E\mathbf{S}_{CR} - \mathbf{H}_{CR})\mathbf{G}_{RC} = \mathbf{I}_{CC} \tag{3.33}$$

$$(E\mathbf{S}_{LC} - \mathbf{H}_{LC})^{\dagger}\,\mathbf{G}_{LR} + (E\mathbf{S}_{CC} - \mathbf{H}_{CC})\mathbf{G}_{CR} + (E\mathbf{S}_{CR} - \mathbf{H}_{CR})\mathbf{G}_{RR} = \mathbf{0} \tag{3.34}$$

$$(E\mathbf{S}_{CR} - \mathbf{H}_{CR})^{\dagger}\mathbf{G}_{CL} + (E\mathbf{S}_{RR} - \mathbf{H}_{RR})\mathbf{G}_{RL} = \mathbf{0} \tag{3.35}$$

$$(E\mathbf{S}_{CR} - \mathbf{H}_{CR})^{\dagger}\mathbf{G}_{CC} + (E\mathbf{S}_{RR} - \mathbf{H}_{RR})\mathbf{G}_{RC} = \mathbf{0} \tag{3.36}$$

$$(E\mathbf{S}_{CR} - \mathbf{H}_{CR})^{\dagger}\mathbf{G}_{CR} + (E\mathbf{S}_{RR} - \mathbf{H}_{RR})\mathbf{G}_{RR} = \mathbf{I}_{RR} \tag{3.37}$$

Equation (3.30) results in:

$$(E\mathbf{S}_{LL} - \mathbf{H}_{LL})\mathbf{G}_{LC} = -(E\mathbf{S}_{LC} - \mathbf{H}_{LC})\mathbf{G}_{CC} \tag{3.38}$$

$$\mathbf{G}_{LC} = -(E\mathbf{S}_{LL} - \mathbf{H}_{LL})^{-1}(E\mathbf{S}_{LC} - \mathbf{H}_{LC})\mathbf{G}_{CC} \tag{3.39}$$

Also similarly Equation (3.36) gives:

$$(E\mathbf{S}_{CR} - \mathbf{H}_{CR})^{\dagger}\mathbf{G}_{CC} = -(E\mathbf{S}_{RR} - \mathbf{H}_{RR})\mathbf{G}_{RC} \tag{3.40}$$

$$\mathbf{G}_{RC} = -(E\mathbf{S}_{RR} - \mathbf{H}_{RR})^{-1}(E\mathbf{S}_{CR} - \mathbf{H}_{CR})^{\dagger}\mathbf{G}_{CC} \tag{3.41}$$

Using Equation (3.39) and (3.41) in Equation (3.33) yields:

$$\begin{aligned} &-(E\mathbf{S}_{LC} - \mathbf{H}_{LC})^{\dagger}(E\mathbf{S}_{LL} - \mathbf{H}_{LL})^{-1}(E\mathbf{S}_{LC} - \mathbf{H}_{LC})\mathbf{G}_{CC} + (E\mathbf{S}_{CC} - \mathbf{H}_{CC})\mathbf{G}_{CC} \\ &-(E\mathbf{S}_{CR} - \mathbf{H}_{CR})(E\mathbf{S}_{RR} - \mathbf{H}_{RR})^{-1}(E\mathbf{S}_{CR} - \mathbf{H}_{CR})^{\dagger}\mathbf{G}_{CC} = \mathbf{I}_{CC} \end{aligned} \tag{3.42}$$

$$\begin{aligned} &\Big[(E\mathbf{S}_{CC} - \mathbf{H}_{CC}) - (E\mathbf{S}_{LC} - \mathbf{H}_{LC})^{\dagger}(E\mathbf{S}_{LL} - \mathbf{H}_{LL})^{-1}(E\mathbf{S}_{LC} - \mathbf{H}_{LC}) \\ &-(E\mathbf{S}_{CR} - \mathbf{H}_{CR})(E\mathbf{S}_{RR} - \mathbf{H}_{RR})^{-1}(E\mathbf{S}_{CR} - \mathbf{H}_{CR})^{\dagger}\Big]\mathbf{G}_{CC} = \mathbf{I}_{CC} \end{aligned} \tag{3.43}$$

Since $\mathbf{S}_{CR}$ and $\mathbf{H}_{CR}$ matrices are hermitian, one can write

$$(E\mathbf{S}_{CR} - \mathbf{H}_{CR}) = (E\mathbf{S}_{CR} - \mathbf{H}_{CR})^{\dagger} \tag{3.44}$$

Using Equation (3.44) in Equation (3.43) gives:

$$\begin{aligned} &\Big[(E\mathbf{S}_{CC} - \mathbf{H}_{CC}) - (E\mathbf{S}_{LC} - \mathbf{H}_{LC})^{\dagger}(E\mathbf{S}_{LL} - \mathbf{H}_{LL})^{-1}(E\mathbf{S}_{LC} - \mathbf{H}_{LC}) \\ &-(E\mathbf{S}_{CR} - \mathbf{H}_{CR})^{\dagger}(E\mathbf{S}_{RR} - \mathbf{H}_{RR})^{-1}(E\mathbf{S}_{CR} - \mathbf{H}_{CR})\Big]\mathbf{G}_{CC} = \mathbf{I}_{CC} \end{aligned} \tag{3.45}$$

Also the Green's function equation for the left and right leads, respectively are given by;

$$E\mathbf{S}_{LL} - \mathbf{H}_{LL} = I_{LL}$$

$$(E\mathbf{S}_{LL} - \mathbf{H}_{LL})^{-1} = \mathbf{G}_{LL} \tag{3.46}$$

$$E\mathbf{S}_{RR} - \mathbf{H}_{RR} = I_{RR}$$

$$(E\mathbf{S}_{RR} - \mathbf{H}_{RR})^{-1} = \mathbf{G}_{RR} \tag{3.47}$$

Using Equation (3.46) and (3.47) in Equation (3.45) yields:

$$\begin{aligned}&\Big[(E\mathbf{S}_{CC} - \mathbf{H}_{CC}) - (E\mathbf{S}_{LC} - \mathbf{H}_{LC})^{\dagger}\,\mathbf{G}_{LL}\,(E\mathbf{S}_{LC} - \mathbf{H}_{LC}) \\ &- (E\mathbf{S}_{CR} - \mathbf{H}_{CR})^{\dagger}\mathbf{G}_{RR}\,(E\mathbf{S}_{CR} - \mathbf{H}_{CR})]\,\mathbf{G}_{CC} = \mathbf{I}_{CC}\end{aligned} \tag{3.48}$$

Self energies of the left and right leads are defined by, respectively:

$$\mathbf{\Sigma}_L = (E\mathbf{S}_{LC} - \mathbf{H}_{LC})^{\dagger}\mathbf{G}_{LL}(E\mathbf{S}_{LC} - \mathbf{H}_{LC}) \tag{3.49}$$

$$\mathbf{\Sigma}_R = (E\mathbf{S}_{CR} - \mathbf{H}_{CR})^{\dagger}\mathbf{G}_{RR}(E\mathbf{S}_{CR} - \mathbf{H}_{CR}) \tag{3.50}$$

The self-energies contain the information on which states are available in the leads at a given energy. Electrons can propagate from the scattering region into these available states. (See Figure 3.3) Using Equation (3.49) and (3.50) in Equation (3.48) results:

$$[((E\mathbf{S}_{CC} - \mathbf{H}_{CC}) - \mathbf{\Sigma}_L - \mathbf{\Sigma}_R]\mathbf{G}_{CC} = \mathbf{I}_{CC} \tag{3.51}$$

Green's function of the scattering region is found as:

$$\mathbf{G}_{CC} = \{E\mathbf{S}_{CC} - [\mathbf{H}_{CC} + \mathbf{\Sigma}_L + \mathbf{\Sigma}_R]\}^{-1} \tag{3.52}$$

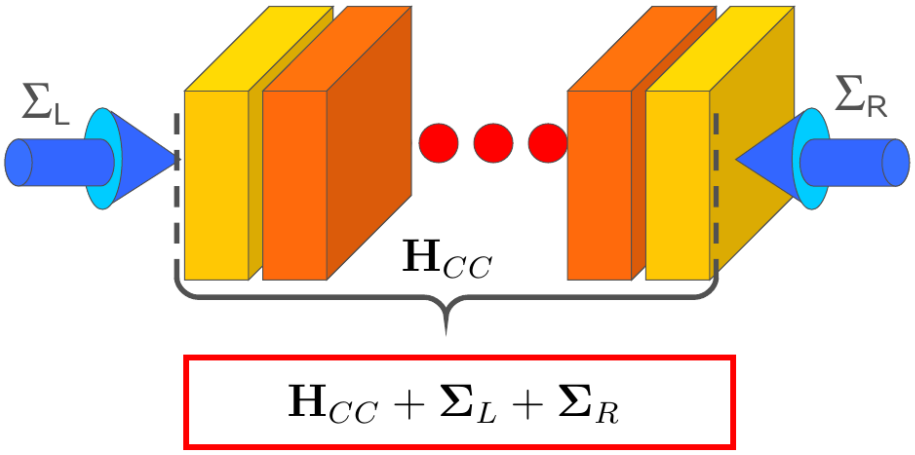

Figure 3.3. Representation of self energies instead of periodic semi-infinite electrodes. (Source: [131])

There are two solution for this equation. First one is advanced and second one is retarded. Replacing E with $E + i\eta$ ensures the only solution is retarded Green's function. Green's function can easily be obtained since we know all the quantities on the opposite side of the equation.

3.4.2. Current Calculation

Landauer type electron transport states that there are two kind of scattering states in the scattering region which they come from left and right leads. The left (right) electrode's scattering states with energy below μ_L (μ_R) are occupied. The chemical potentials of both leads are same while there is no bias. Thus the contributions from the both leads' states counteracts each other, leading to zero net current. However when a bias applied to the system across to the junction, equilibrium state no longer exists and leading to non-zero current. In this context, self-consistent method is necessary to evaluation of current since the occupations of each scattering states would be affected by the non-equilibrium boundary condition (see Figure 3.4). Under zero bias density matrix is obtained as

$$\rho = \frac{1}{2\pi i} \int dE\, i \left[\mathbf{G}_{CC} \mathbf{\Gamma}_L \mathbf{G}_{CC}^{\dagger} f(E - \mu_L) + \mathbf{G}_{CC} \mathbf{\Gamma}_R \mathbf{G}_{CC}^{\dagger} f(E - \mu_R) \right] \tag{3.53}$$

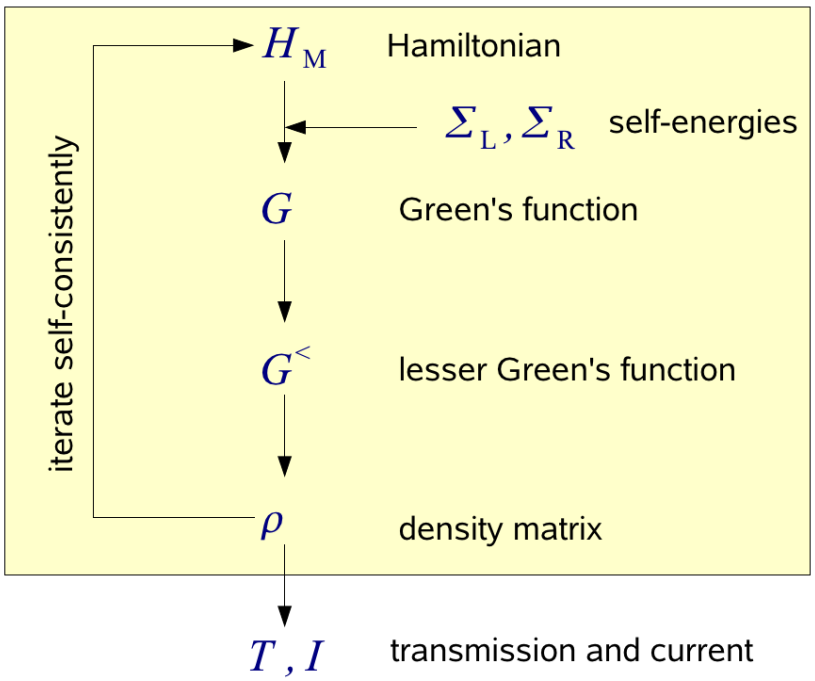

Figure 3.4. A schematic representation of self-consistent method for NEGF+DFT. (Source: [131])

where $\mathbf{\Gamma}_{L(R)}$ represents the coupling between the electrodes and scattering region and they introduce broadening of the molecular levels,

$$\mathbf{\Gamma}_{L(R)} = i\,(\mathbf{\Sigma_{L(R)}} - \mathbf{\Sigma_{L(R)}}^{\dagger}) \tag{3.54}$$

and f is Fermi-Dirac distribution function. Moreover lesser Green's function is defined as

$$\mathbf{G}^{<} = i\,\mathbf{G}_{CC}[f(E-\mu_L)\mathbf{\Sigma_L} + f(E-\mu_R)\mathbf{\Sigma_R}]\mathbf{G}_{CC}^{\dagger} \tag{3.55}$$

Using the Equation (3.55) in (3.53) results

$$\rho = \frac{1}{2\pi i}\int dE\, i\,\mathbf{G}^{<} \tag{3.56}$$

The density matrix can be feed back to DFT modules to generate new ground state density which leads to calculation of Hamiltonian $\mathbf{H}_{CC}$ thus a new iteration starts from the calculation of new Green's function, and iterates until convergence is achieved. Then the

current can be calculated by:

$$I = \frac{e}{h} \int dE\, T(E)\, [f(E - \mu_L) - f(E - \mu_R)]$$

$$I \approx \frac{e}{h} \int_{\mu_R}^{\mu_L} dE\, T(E) \tag{3.57}$$

where $T(E)$ is the transmission probability of injecting electrons with energy E. Transmission function can be calculated directly from the Green's function of the scattering region

$$T(E) = \mathbf{Tr}[\mathbf{\Sigma}_L \mathbf{G}_{CC} \mathbf{\Sigma}_R \mathbf{G}_{CC}^{\dagger}] \tag{3.58}$$

Under non-zero bias the density and current equations becomes

$$\rho^{\sigma} = \frac{1}{2\pi} \int dE\, [\mathbf{G}_{CC} \mathbf{\Sigma}_L f(E, \mu_L) \mathbf{G}_{CC}^{\dagger} + \mathbf{G}_{CC} \mathbf{\Sigma}_R f(E, \mu_R) \mathbf{G}_{CC}^{\dagger}]_{ij}^{\sigma} \tag{3.59}$$

$$I^{\sigma} = \frac{e}{h} \int dE\, [\mathbf{Tr}(\mathbf{\Sigma}_L \mathbf{G}_{CC} \mathbf{\Sigma}_R \mathbf{G}_{CC}^{\dagger})(f(E, \mu_L) - f(E, \mu_R))]^{\sigma} \tag{3.60}$$

where $\mu_L = E_f + \frac{eV}{2}$ and $\mu_R = E_f - \frac{eV}{2}$. Here E_f is Fermi energy of the leads and V is applied bias.

CHAPTER 4

COBALT-BENZENE NANOWIRE

Molecular magnets has become of interest for research in high-density information storage, quantum computing and spintronics [132]. In this context, among such novel systems Cobalt-Benzene organo-metallic molecule and it's nanowire are studied for possible novel properties.

4.1. Method

First principles density functional theory calculations are carried out using norm-conserving pseudopotentials in their fully nonlocal form and the PBE GGA functional within the SIESTA software package. A double-ζ polarized basis set composed of numerical atomic orbitals of finite range. Convergence tests are performed for k-point sampling scheme and mesh cutoff energy. The electrostatic potentials were determined on a real-space grid with a mesh cutoff energy of 500 Ry. The Brillouin zone has been sampled with (1,1,9) points within the Monkhorst-Pack k-point sampling scheme. For geometry optimizations, a local relaxation has been performed using the conjugate gradient algorithm and the convergence criteria of 0.04 eV$\times$Å^{-1} and 10^{-4} eV for the forces and total energies, respectively, in the self-consistency cycles. Nanowire's periodicity is established in z-direction and vacuum regions of $\sim$ 10 Å is used in both x- and y-directions.

4.2. Results

4.2.1. Geometric Structure

Unit cell of Cobalt-Benzene nanowire can be seen in Figure 4.1. Two different geometric alignment for benzene rings are shown in Figure 4.2; these are, cobalt atoms with staggered benzene rings where the staggering angle is 30^0 and cobalt atoms with not staggered benzene rings. After the geometry optimizations, benzene rings conserved the plane geometry in staggered and not staggered cases. Also Cobalt atoms are perfectly

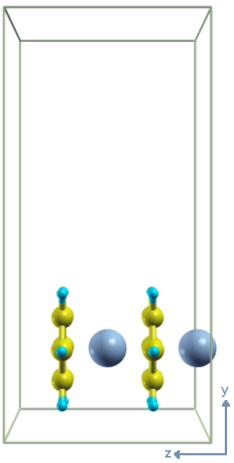

Figure 4.1. Unit Cell and geometric structure of a Cobalt-Benzene nanowire.

placed between the benzene rings. Two different magnetic moment distribution on Cobalt

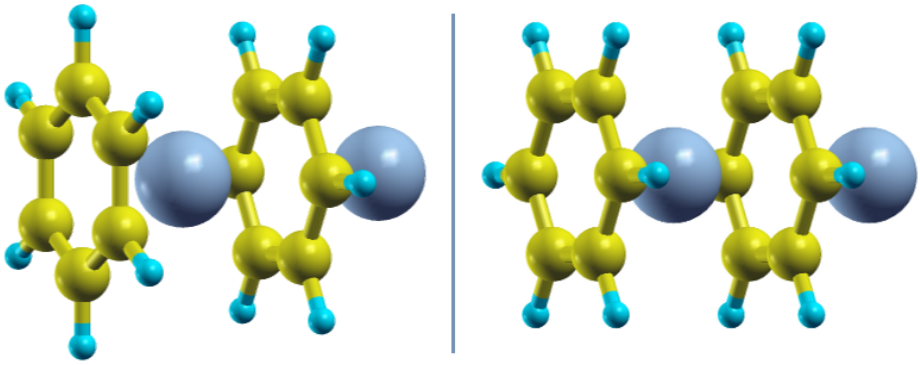

Figure 4.2. Optimized structures for Cobalt-Benzene nanowire: (a) Second Benzene ring is rotated 30 degrees respect to first Benzene ring in x-y plane (staggered) , (b) None of the Benzene are rings rotated (not staggered).

atoms are considered which are, the cobalt atoms' magnetic moments' direction is opposite with respect to the neighbor cobalt atoms (antiferromagnetic) and the all cobalt atoms' magnetic moments' are aligned to the same direction (ferromagnetic) for both staggered and not staggered geometries of benzene rings. Unit cell relaxation along the z-direction is performed for ferromagnetic/antiferromagnetic and staggered/not staggered case (see Figure 4.3).

Bond lengths and total energies of optimized geometries are given in table 4.1 for all ferromagnetic/antiferromagnetic and staggered/not staggered cases. Cobalt-Benzene nanowire with not staggered geometry and ferromagnetic order has lowest total energy. Also C-C and C-H lengths are same for ferromagnetic and staggered; antiferromagnetic

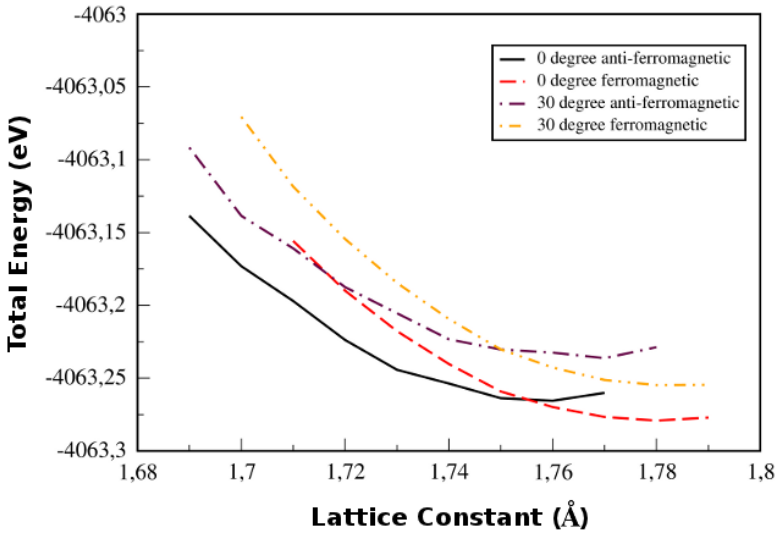

Figure 4.3. Unit cell relaxation results for each case.

Table 4.1. Bond lengths and total energies of Cobalt-Benzene nanowires.

System Name	C-C Bond Length (Å)	C-H Bond Length (Å)	C-Co Bond Length (Å)	Total Energy (eV)
Not staggered Ferromagnetic	1.43	1.1	2.28	-4061.978
Not staggered Anti-ferromagnetic	1.43	1.1	2.27	-4061.972
Staggered Ferromagnetic	1.43	1.1	2.28	-4061.977
Staggered Anti-ferromagnetic	1.43	1.1	2.29	-4061.882

and staggered; ferromagnetic and not staggered; antiferromagnetic and not staggered cases meanwhile C-Co bond length is slightly changing.

4.2.2. Electronic Properties

Figure 4.4-4.7 represent the energy band and DOS diagram for ferromagnetic/ antiferromagnetic and staggered/not staggered case. Each case modifies the electronic properties of Cobalt-Benzene nanowire differently. As seen in Figure 4.5 and 4.7, the systems with ferromagnetic ordering have only one flat band of minority spin component crossing Fermi level while there is no band of the majority spin component crossing Fermi level, thus resulting band gaps 0.67 eV and 0.62 eV for not staggered and staggered cases, respectively. In the antiferromagnetic cases (see Figure 4.4 and 4.6), there are bands which passing Fermi level with spin degeneracy. Thus the antiferromagnetic systems are

metallic.

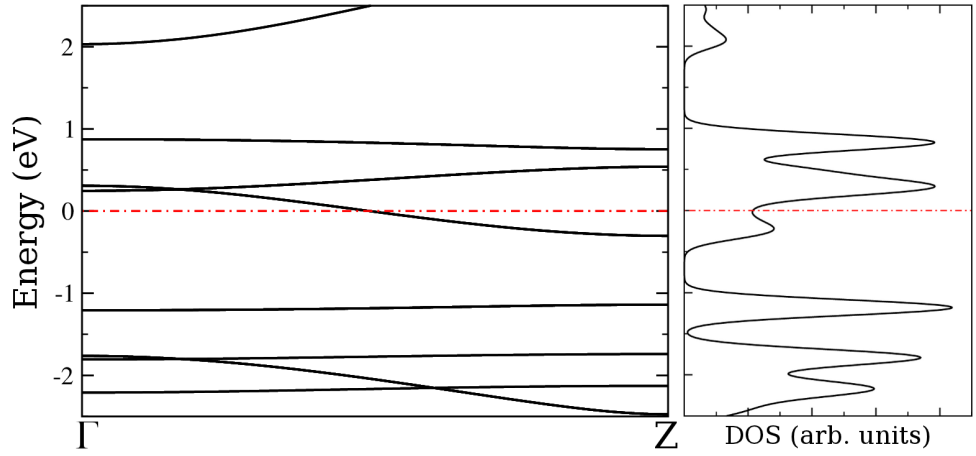

Figure 4.4. Band structure and DOS diagram for the not staggered and antiferromagnetic system. Spin degenerate case. Fermi level shifted to 0.

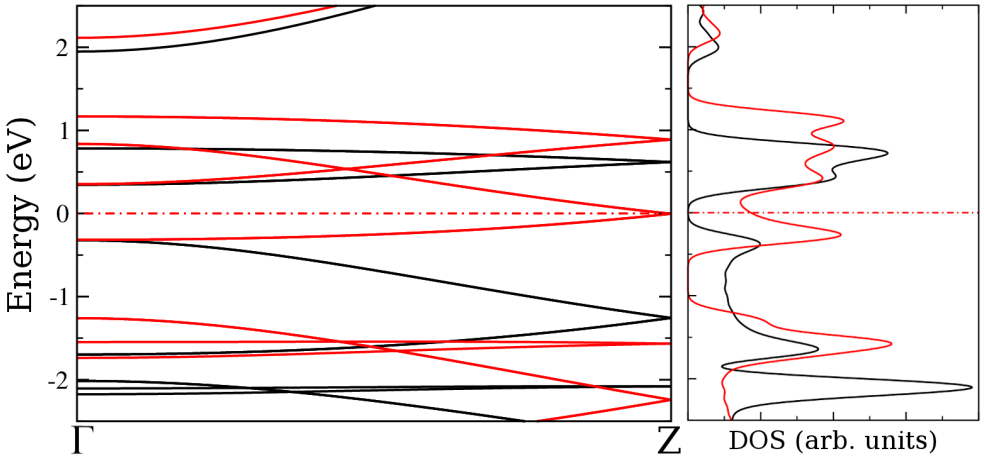

Figure 4.5. Band structure and DOS diagram for the not staggered and ferromagnetic system. Black lines represent the majority spin while red lines represent minority spin. Fermi level shifted to 0.

The van-Hove singularities are present in the DOS plots of staggered/not staggered and ferromagnetic/antiferromagnetic systems which characteristic to one-dimensional systems (see Figure 4.4-4.7). The DOS plots of the ferromagnetic staggered (Figure 4.7) and ferromagnetic not staggered (Figure 4.5) systems display spin non-degenerate curves. The energy band gap for the majority spin channel is present as expected while minority spin component of density is not vanishing at Fermi level at the ferromagnetic staggered and ferromagnetic not staggered cases. In contrary to the ferromagnetic systems, antiferromagnetic staggered and antiferromagnetic not staggered systems have spin degenerate DOS plots but with not vanishing DOS at Fermi level (see Figure 4.4 and Fig 4.6).

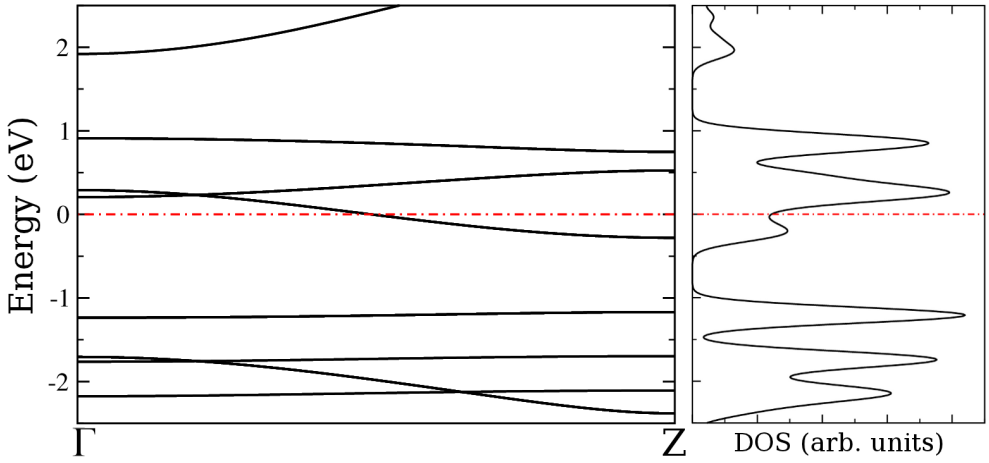

Figure 4.6. Band structure and DOS diagram for the staggered and antiferromagnetic system. Spin degenerate case. Fermi level shifted to 0.

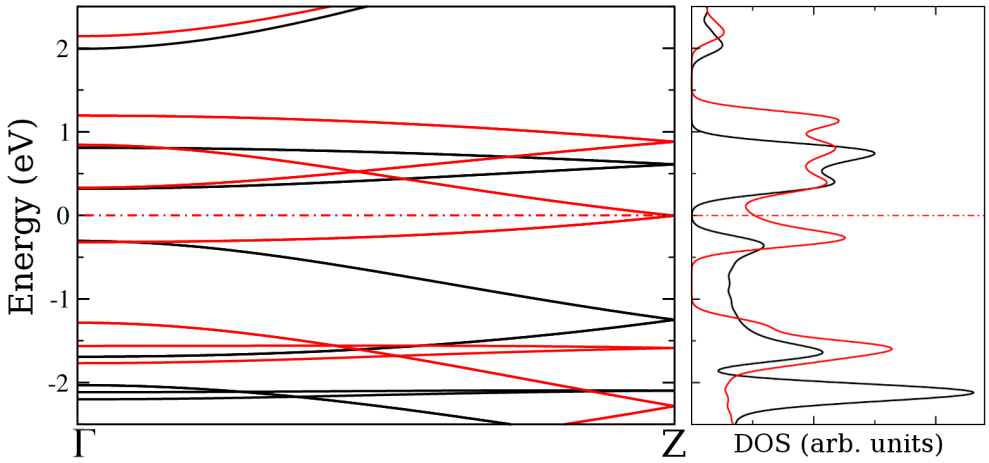

Figure 4.7. Band structure and DOS diagram for the staggered and ferromagnetic system. Black lines represent the majority spin while red lines represent minority spin. Fermi level shifted to 0.

4.2.3. Magnetic Properties

The spin-dependent charge densities of the optimized structures and their difference ($\Delta\rho = \rho_{\uparrow} - \rho_{\downarrow}$) are calculated. The spin states are localized on Co atoms (see Fig 4.8-4.9). Using Mulliken population analysis spin dependent atomic charges, total valance charge and the spin magnetic moments of the atoms are determined. Total magnetic moments, total charge of the atoms, and induced magnetic moments of the atoms for staggered/not staggered and antiferromagnetic/ferromagnetic cases are given in table 4.2. As seen in the figures 4.8-4.9, there are no net induced magnetic moments on the C and H atoms either. When a Co atom binds to Benzene ring, the valance charges of the C and H

atoms are partially transferred to the Co atom due to higher electron affinity of Co than the benzene molecule [133]. As it is seen in table 4.2, transferred total charges per atom to Co atoms are 0.209, 0.182, 0.175, 0.168 for not staggered and antiferromagnetic, staggered and antiferromagnetic, staggered and ferromagnetic, not staggered and ferromagnetic, respectively. This charge transfer results indicates that the systems with antiferromagnetic ordering tend to accept more charge from benzene rings compared to the systems with ferromagnetic ordering resulting smaller magnitude of the magnetic moments on Co atoms.

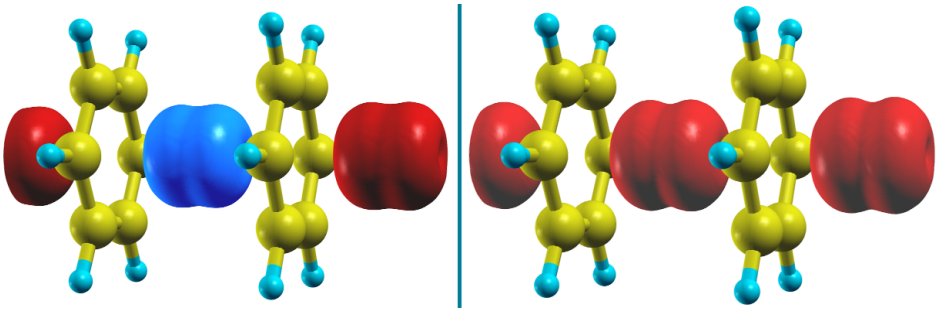

Figure 4.8. Relaxed geometric structure and isosurfaces of charge density difference of spin-up (↑) and spin-down (↓) states for not staggered and antiferromagnetic (left), not staggered and ferromagnetic (right). For all geometries, positive and negative values of the charge density difference is shown by red and blue regions, respectively, for the same isosurface value of ± 0.002 electrons/Å^3.

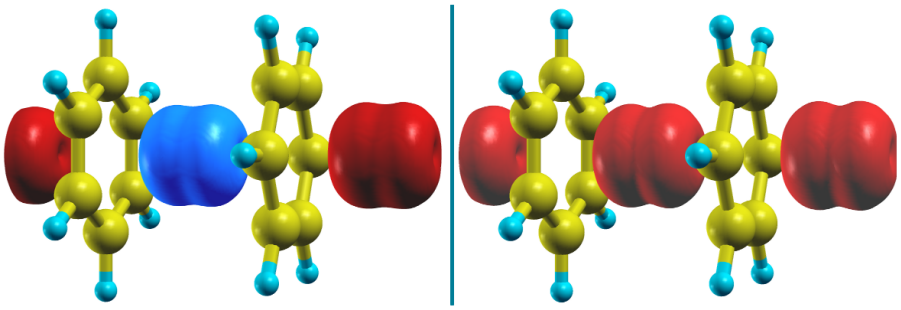

Figure 4.9. Relaxed geometric structure and isosurfaces of charge density difference of spin-up (↑) and spin-down (↓) states for staggered and antiferromagnetic (left), staggered and ferromagnetic (right). For all geometries, positive and negative values of the charge density difference is shown by red and blue regions, respectively, for the same isosurface value of ± 0.002 electrons/Å^3.

Table 4.2. Total valance charge and the spin magnetic moments of the atoms for Cobalt-Benzene nanowires.

	Total Charges			Magnetic Moments (μ_B)		
System Name	**C**	**H**	**Co**	**Co_1**	**Co_2**	Total
Not staggered Ferromagnetic	3.739	1.233	9.168	1.032	1.032	2
Not staggered Anti-ferromagnetic	3.732	1.232	9.209	0.729	-0.729	0
Staggered Ferromagnetic	3.736	1.234	9.175	1.023	1.023	2
Staggered Anti-ferromagnetic	3.736	1.234	9.182	0.772	-0.772	0

4.2.4. Transport Properties

As a small part of the cobalt-benzene nanowire, $Co_3(Bz)_2$ molecule is used to calculate of transmission and current (see Figure 4.10). 3-dimensional gold crystals are used as electrodes. Electrode surface is chosen as (1,1,1) direction of gold crystal. Self energies of gold electrodes are calculated separately and included into the current calculation. Some portion of the gold electrodes are included into molecule from both sides due to avoid direct interactions between the electrodes they form scattering regions (see Figure 4.11). After the geometric relaxations for the scattering regions three systems are obtained: (1) Not-staggered antiferromagnetic , (2) Not-staggered ferromagnetic , (3) Staggered antiferromagnetic.

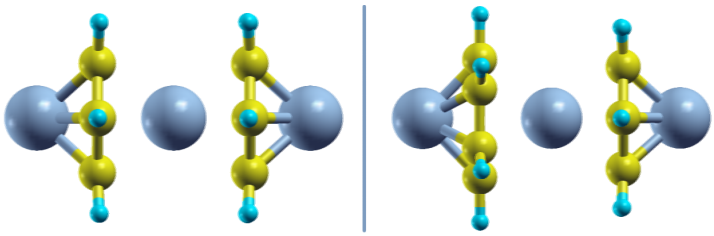

Figure 4.10. $Co_3(Bz)_2$ molecule. Left: Not staggered case. Right: Staggered case.

During the calculation of the current and transmission, in order to match the device potential and the surface potential of the semi-infinite gold electrodes, additionally some more portion of the gold electrodes are included into the device region (see Figure 4.12). These additionally included parts of the gold electrodes are kept fixed during the geometric optimizations of the large supercells of scattering regions.

Results of ab-initio electron transport calculations of not staggered geometry with

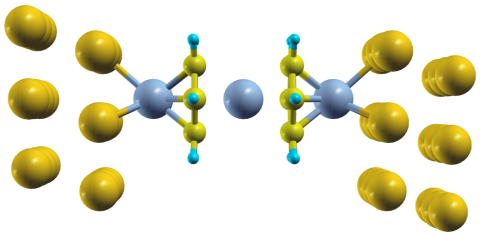

Figure 4.11. $Co_3(Bz)_2$ molecule is with some small part of the electrodes which they form scattering region.

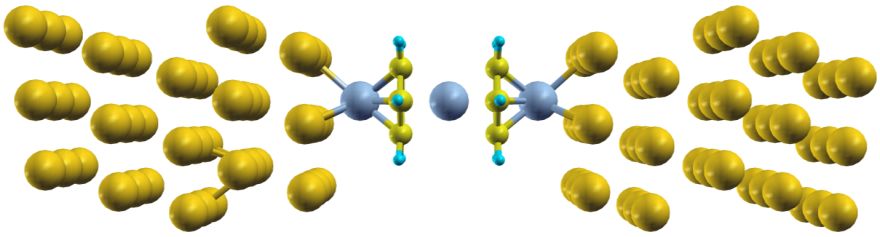

Figure 4.12. $Co_3(Bz)_2$ molecule is with small and an extra part of the electrodes for current calculation.

antiferromagnetic and ferromagnetic ordering and staggered geometry with anti- ferromagnetic ordering of $Co_3(Bz)_2$ molecule are given in Figure 4.13 and 4.14. Spin polarized currents are obtained in all cases.

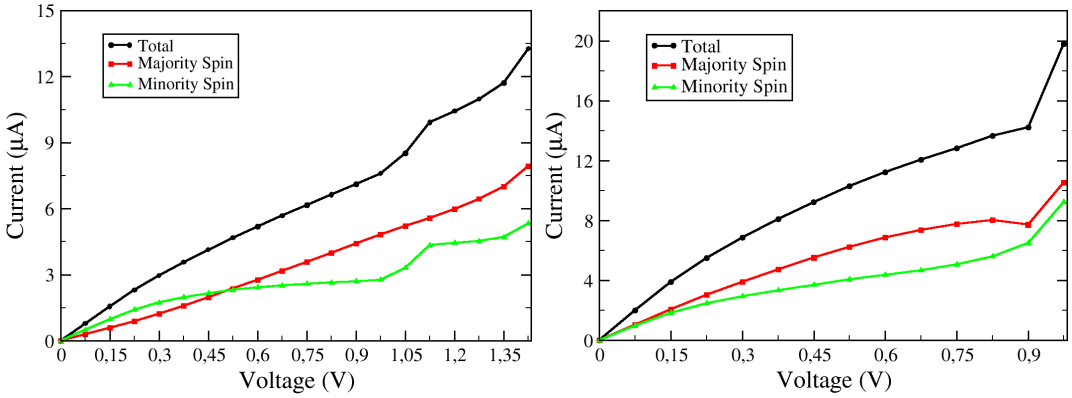

Figure 4.13. Current calculation results respect to applied bias for not staggered cases. Left: not staggered and antiferromagnetic. Right: not staggered and ferromagnetic.

The spin polarization of the current is defined as $[(I_\uparrow - I_\downarrow) / (I_\uparrow + I_\downarrow)]$ and given in right side of the Figure 4.14 for not staggered geometry with antiferromagnetic and ferromagnetic ordering and staggered geometry with antiferromagnetic ordering . In this figure, the spin polarization ratio of the current has always a positive value for the not staggered and ferromagnetic case. Thus one component of the spin in the current is al-

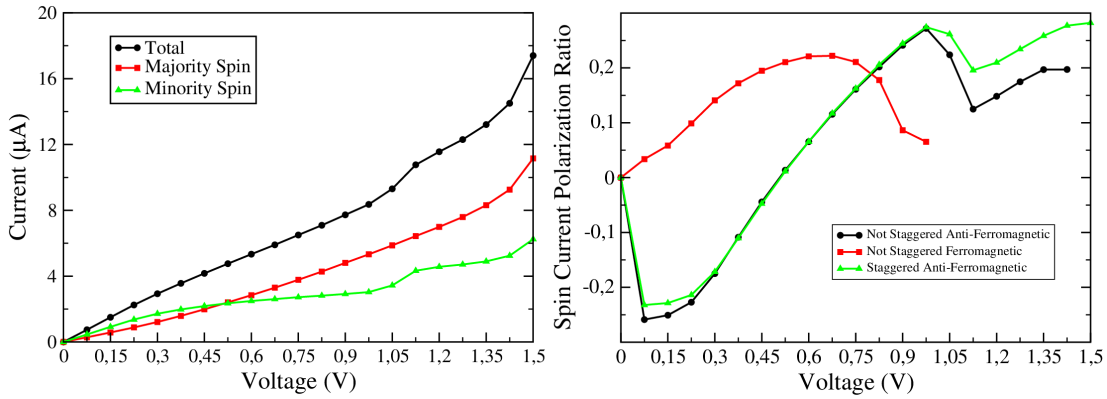

Figure 4.14. Left: Current calculation results respect to applied bias for staggered case with antiferromagnetic ordering. Right: Spin polarized current ratio versus applied bias voltage for each three cases.

ways dominant in the full range of the applied bias. On the other hand the systems with antiferromagnetic ordering have a changing value between the negative and positive values of spin polarization ratio of the current. Therefore the one component of the spin in the current is dominant up to the applied bias voltage of 0.5 V while other component of the spin is dominant from 0.5 V to 1.5 V.

CHAPTER 5

ALKALI ATOM-TERMINATED ZIGZAG GRAPHENE NANORIBBONS

In order to manipulate the electronic properties of ZGNRs, modification [134, 135] and functionalization [136] of edges and producing defects, doping [137–140] and absorbtion [141–143] of atoms or molecules on ZGNRs have been extensively studied. For instance, recent studies [144, 145] have shown ways to obtain half-metallic ZGNRs. In this context, edge functionalization of ZGNR with alkali atoms are studied for possible novel properties.

5.1. Method

First principles density functional theory calculations are carried out using norm-conserving pseudopotentials in their fully nonlocal form and the PBE GGA functional within the SIESTA software package. A double-ζ polarized basis set composed of numerical atomic orbitals of finite range. Convergence tests are performed for k-point sampling scheme and mesh cutoff energy. The electrostatic potentials were determined on a real-space grid with a mesh cutoff energy of 300 Ry. The Brillouin zone has been sampled with (1,1,70) points within the Monkhorst-Pack k-point sampling scheme. For geometry optimizations, a local relaxation has been performed using the conjugate gradient algorithm and the convergence criteria of 0.04 eV$\times$Å^{-1} and 10^{-4} eV for the forces and total energies, respectively, in the self-consistency cycles. Nanowire's periodicity is established in z-direction and vacuum regions of $\sim$ 10 Å is used in both x- and y-directions.

5.2. Results

5.2.1. Geometric Structure

Zigzag graphene nanoribbons (ZGNR) with different widths are geometrically optimized using geometry and unit cell that is shown in Figure 5.1. Ribbon width change

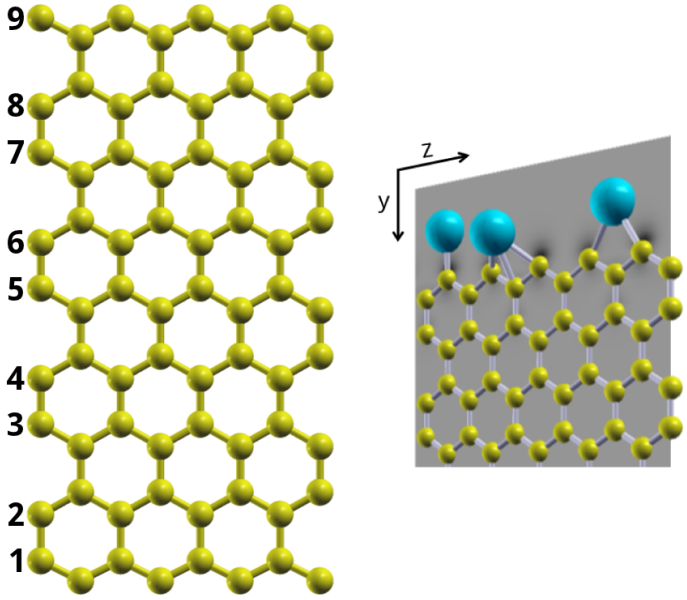

Figure 5.1. Left: Unit Cell and geometric structure of zigzag graphene nanoribbon. Right: Schematic representation of various binding geometries of alkali atoms to a ZGNR edge. From left to right: top in-plane (TI), bridge off-plane (BO), bridge in-plane (BI).

is parameterized in left side of the Figure 5.1. The geometric relaxation calculations is done for different ribbon width N-ZGNR (N=5,6,7,8,9). In this study edge termination of n-ZGNRs (n denoting the number of zigzag rows in the ribbon) with monovalent atoms, i.e. H, Li, Na and K are considered. In the right side of the Figure5.1, different binding geometries of monovalent atoms to ZGNR determined after geometry optimizations are shown; these are, on top of an edge C atom, in-plane with the ribbon (TI); bridge site of two edge C atoms, either off-plane (BO), or in plane (BI). Unlike H-termination, Li, Na, K atoms prefer to bind at the bridge sites rather than the TI site. Binding energy is defined as,

$$E_B = |E_{tot} - E_{pri} - (n \cdot E_{atom})|/n \tag{5.1}$$

where E_{tot} is total energy of the alkali atom adsorbed into NZGNR, E_{pri} is total energy of the pristine NZGNR, E_{atom} is the total energy energy of the alkali atom only and n is the total number of alkali atoms in the unit cell. Binding energies of single Li, Na, K atoms at a BI sites and TI sites of the 9ZGNR are given in table 5.1. Two different concentrations of Li, Na, K atoms for saturation of the edges are considered which they are, full coverage (FC) where there are as many Li, Na, K atoms as the edge C atoms, and

Table 5.1. Bond lengths, vertical distances, and binding energies of Li, Na, and K terminated 9ZGNR.

9ZGNR	Alkali atom-Carbon Bond Length (Å)	Vertical Distance (Å)	Binding Energy (eV)
Li (HC)	2.00	0	3.711
Li (FC)	2.00	0.88	3.550
Na (HC)	2.33	0	3.115
Na (FC)	2.34	1.22	2.786
K (HC)	2.66	0.22	3.218
K (FC)	2.73	1.72	2.600

Table 5.2. Bond lengths, vertical distances, and binding energies of Li, Na, and K terminated at HC with 5ZGNR, 6ZGNR, 7ZGNR, 8ZGNR.

	Alkali atom-Carbon Bond Length (Å)	Vertical Distance (Å)	Binding Energy (eV)
Li (5ZGNR)	1.99	0	3.637
Li (6ZGNR)	2.00	0	3.686
Li (7ZGNR)	2.00	0	3.698
Li (8ZGNR)	2.00	0	3.706
Na (5ZGNR)	2.33	0	2.932
Na (6ZGNR)	2.33	0	2.984
Na (7ZGNR)	2.33	0	3.031
Na (8ZGNR)	2.33	0	3.074
K (5ZGNR)	2.66	0.42	2.808
K (6ZGNR)	2.66	0.28	2.910
K (7ZGNR)	2.66	0.20	3.016
K (8ZGNR)	2.66	0.19	3.118

half coverage (HC) where the Li, Na, K atoms are bound to every other bridge site only (see Figure5.10 (b) for the unit cell of the ribbon and Na binding sites). The bond lengths of the monovalent atom-carbon for the HC cases with Li, Na, K are given in table 5.1. Also edge termination of ZGNR with Li, Na, and K atoms at HC is studied for 5ZGNR, 6ZGNR, 7ZGNR, and 8ZGNR and the bond lengths with vertical distances are given in table 5.2. As it seen in table 5.2, alkali atom-edge carbon atom bond length does not vary with width of the ZGNR while vertical distance of the K atom inversely proportional to the width of the ZGNR. Also the binding energies of the adatoms slightly increases with width of the ZGNNR for all Li, Na, and K cases. In the FC with 9ZGNR case, however, due to their larger atomic size than H, neighboring Li, Na, K atoms relax towards opposite directions at the BO sites. In this case, monovalent atom-carbon bond lengths and vertical distances of Li, Na, K to the plane of ribbon are given in table 5.1.

5.2.2. Electronic Properties

The energy band diagram and density of states of pristine 9ZGNR, Li terminated 9ZGNR at HC and FC, Na terminated 9ZGNR at HC and FC, K terminated 9ZGNR at HC and FC concentrations are displayed in Figure 5.2-5.9, respectively. Each case modifies the electronic properties of the ribbon differently. Pristine 9ZGNR is a semiconductor with a direct band gap of $E_g = 0.70$ eV (see Figure 5.2). Fully hydrogenated 9ZGNR

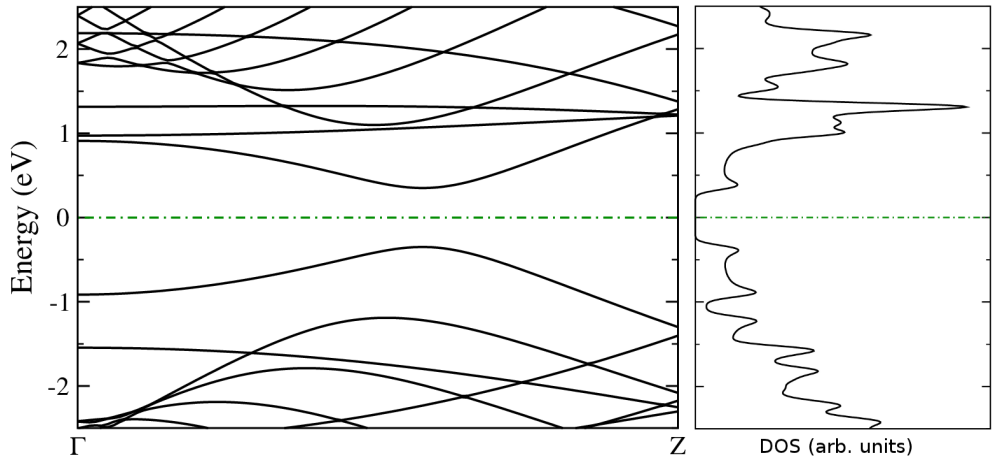

Figure 5.2. Band structure and DOS diagram for the pristine 9ZGNR. Spin degenerate case. Fermi level shifted to 0.

has a lower band gap of $E_g = 0.50$ eV, consistent with a previous report [146]. Similarly, 9ZGNR terminated with Li and Na at FC concentration has a reduced and slightly indirect band gap of $E_g = 0.44$ eV (see Figure 5.3 and 5.4).

At HC concentration of Na termination the 9ZGNR becomes a zero-gap semimetal with an interesting band structure. The valance and conduction bands intersect at a single point. In Figure 5.5, the Dirac-like point is located at $k_0 = 0.469$ Å^{-1} in the first Brillouin zone ($k_Z = 0.625$ Å^{-1}). The tilted Dirac cone is formed by a steep linear band crossing a relatively flat band at the Fermi level. Linear band is derived from carbon p_x and flat band is mainly derived from combination of carbon p_y, s, and p_z orbitals, respectively (see Figure 5.6). Also the states around the Fermi level are localized near the edges of ZGNR (see Figure 5.6) . Since the present ribbon structure is one dimensional, the density of states (DOS) at the Fermi level does not vanish unlike 2D-graphene, and also, singularities characteristic to one-dimensional systems is evident in the DOS plot.

Energy band structures showing Dirac cones are quite rare. 2D-graphene is known for having symmetric and isotropic Dirac cones at corners of the first Brillouin zone. In

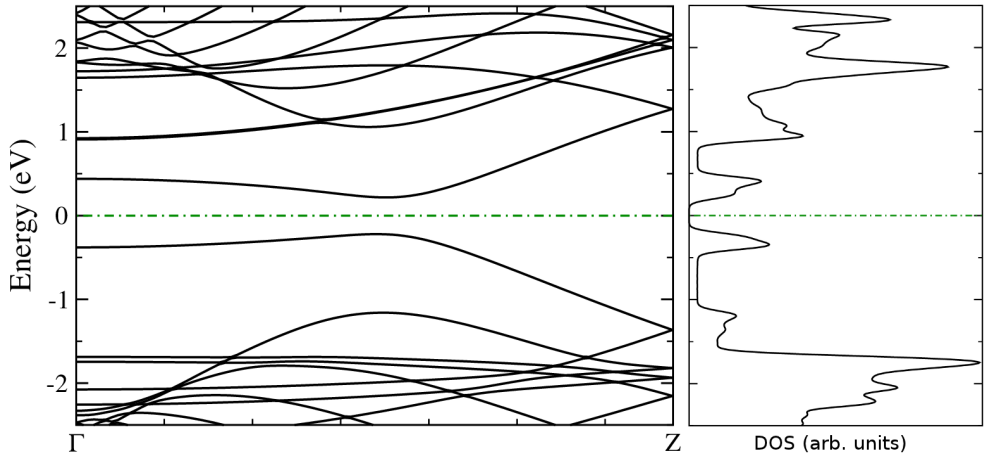

Figure 5.3. Band structure and DOS diagram for the edge termination of 9ZGNR with Li at FC. Spin degenerate case. Fermi level shifted to 0.

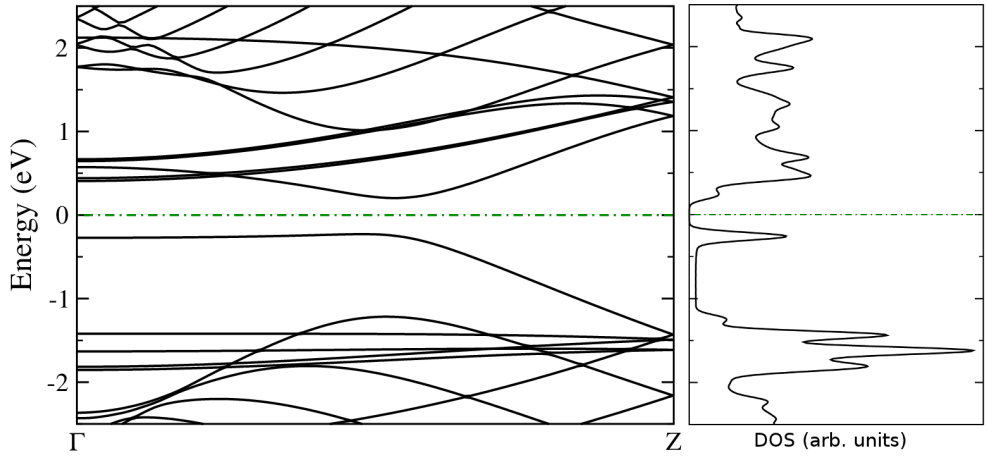

Figure 5.4. Band structure and DOS diagram for the edge termination of 9ZGNR with Na at FC. Spin degenerate case. Fermi level shifted to 0.

this context, recently another two dimensional structure, which is an organic compound, has been reported as a unique material having a gapless band diagram and asymmetrical linear energy dispersion [147]. Na terminated ZGNR at HC concentration that it is presented in this study is a one dimensional member of this class of materials having tilted Dirac "cones". Around the Fermi level, E vs k relation can be approximated in the form,

$$E_\lambda(k) = w_0\,(k - k_0) + \lambda\, w\,|k - k_0| \tag{5.2}$$

where λ plays the role of band index ($+1$ for conduction, and -1 for valance band), $w = 2.517\,\text{eV}\times\text{Å}$ and $w_0 = -2.277\,\text{eV}\times\text{Å}$ are effective velocities. In this representation

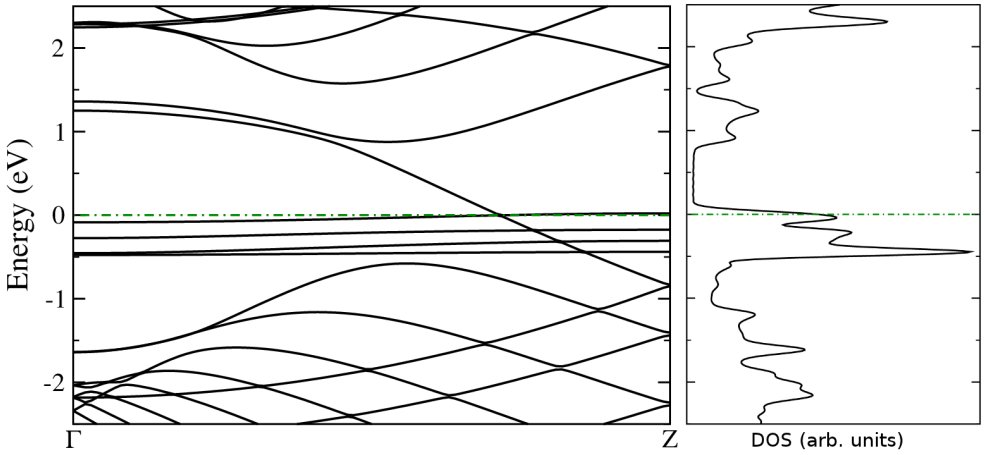

Figure 5.5. Band structure and DOS diagram for the edge termination of 9ZGNR with Na at HC. Spin degenerate case. Fermi level shifted to 0.

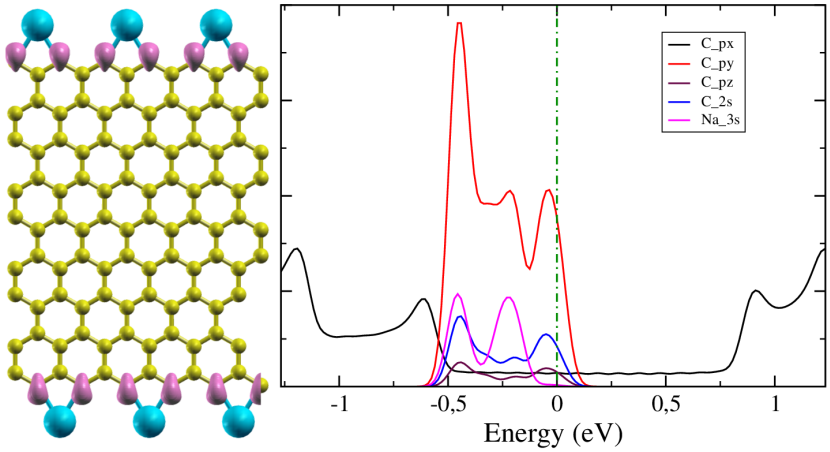

Figure 5.6. Edge termination of 9ZGNR with Na at HC case. Left: Local density of states plot for energy between -1.5 eV and 1.5 eV, isosurface value is 0.05 $Å^{-1}$. Right: Projected density of states plot. Spin degenerate case. Fermi level shifted to 0.

the w_0 parameter determines the degree of tilting of the Dirac cone. The slopes of the bands at the Fermi level are $w_0 + w = 0.240$ eV×Å and $w_0 - w = 4.794$ eV×Å, so that an asymmetry of about a factor of 20 in the slopes of the fermion and antifermion bands is present.

The "tilted Dirac-cone" shaped band structure is quite robust with respect to the ribbon width and the approximations involved, such as exchange correlation functional being LDA or GGA. Also at HC concentration of Li (Figure 5.7), K (Figure 5.8) and FC (Figure 5.9) concentration of K termination produces similar electronic structures, however, the valance and conduction bands intersect at slightly below or above the Fermi energies.

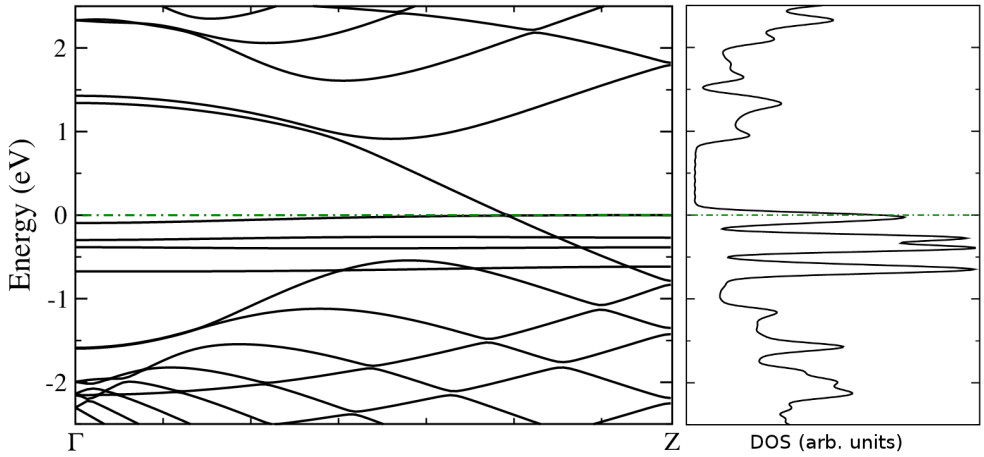

Figure 5.7. Band structure and DOS diagram for the edge termination of 9ZGNR with Li at HC. Spin degenerate case. Fermi level shifted to 0.

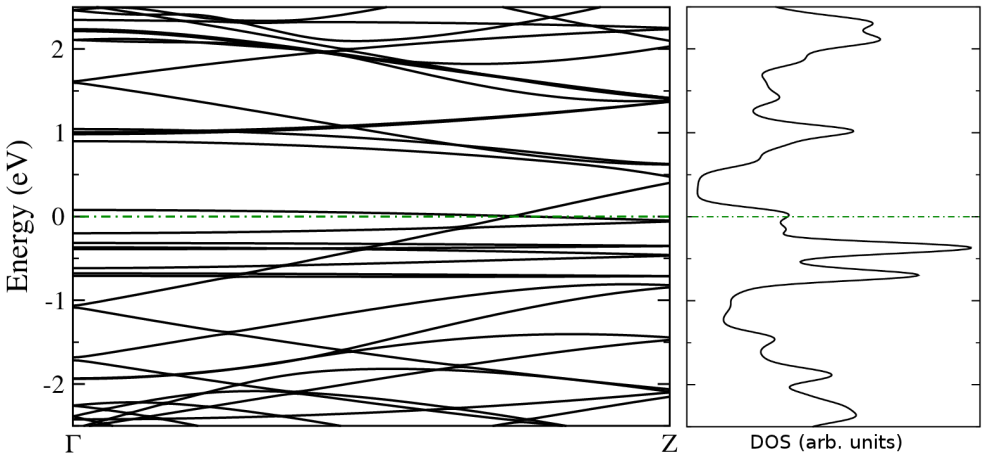

Figure 5.8. Band structure and DOS diagram for the edge termination of 9ZGNR with K at HC. Spin degenerate case. Fermi level shifted to 0.

5.2.3. Magnetic Properties

The spin-dependent charge densities of the optimized structures and their difference ($\Delta\rho = \rho_{\uparrow} - \rho_{\downarrow}$) are calculated.. The characteristic edge-localized spin states of ZGNRs are preserved for both HC and FC concentrations of Li, Na, and K terminated 9-ZGNRS (see Figure5.10-5.11).

Spin dependent atomic charges, total valance charge and the spin magnetic moments of the atoms are determined by using Mulliken population analysis (see table 5.3-5.4). As it seen at table 5.4, total charges and magnetic moments of the edge carbon atoms and Li, Na and K atoms at HC does not vary with the width of the ZGNR. Total magnetic moments of the ribbons are found zero for all cases. As seen in the figures 5.10-5.11, there

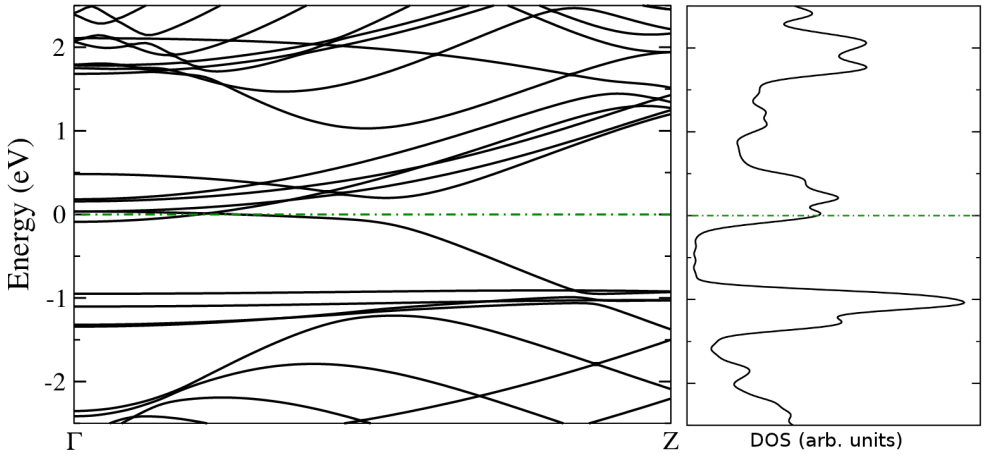

Figure 5.9. Band structure and DOS diagram for the edge termination of 9ZGNR with K at FC. Spin degenerate case. Fermi level shifted to 0.

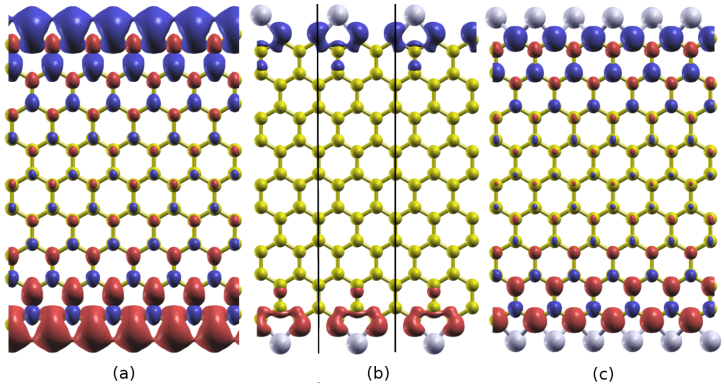

Figure 5.10. Relaxed geometric structure and isosurfaces of charge density difference of spin-up (↑) and spin-down (↓) states for 9-ZGNR; bare (a), and Li terminated at HC (b) and FC (c) concentrations. For all geometries, positive and negative values of the charge density difference is shown by red and blue regions, respectively, for the same isosurface value of ± 0.0025 electrons/Å^3.

are no net induced magnetic moments on the Li, Na, and K atoms either. The penetration of the spin imbalance on the C atoms, $\Delta\rho$, toward the center of ribbons is considerably shorter for the HC cases. Binding of Li, Na, and K atoms reduces the magnetic moments of the edge carbon atoms (see tables 5.3-5.4).

This magnetic moment reduction is comparable to the full hydrogenation of ZGNRs where edge carbon magnetic moments were reported as $\mu = 0.26\,\mu_B$ [148]. When a Li, Na, and K atom binds to ZGNR edge, its valance charge is partially transferred to the ZGNR except at FC of K case where K gains valance charge from ZGNR at FC of K.

This charge transfer towards to the ZGNRs happens due to lower electronegativity of Li, Na, K than C. At HC (FC) concentration, Li and Na atoms transfer 10% (15%) of

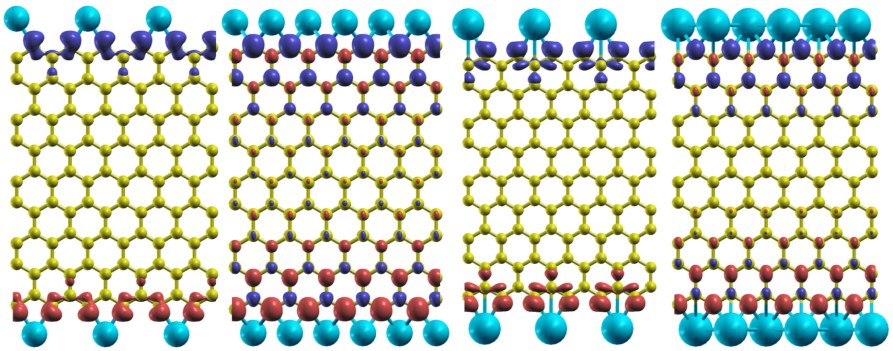

Figure 5.11. Relaxed geometric structure and isosurfaces of charge density difference of spin-up (↑) and spin-down (↓) states for 9-ZGNR; Na terminated at HC (a), FC (b) and K terminated at HC (c) and FC (d) concentrations. For all geometries, positive and negative values of the charge density difference is shown by red and blue regions, respectively, for the same isosurface value of ± 0.0025 electrons/Å^3.

Table 5.3. Total valance charge and the spin magnetic moments of the Li, Na, K at HC and FC with 9ZGNR.

	Total Charges		**Magnetic Moments** (μ_B)	
	Edge C	**Adatom**	**Edge C**	**Adatom**
Pristine	4.06	-	1.21	-
Li(HC)	4.12	0.91	0.10	0.03
Li(FC)	4.23	0.84	0.26	0
Na(HC)	4.13	0.89	0.13	0
Na(FC)	4.21	0.84	0.27	0.01
K(HC)	4.17	0.80	0.15	0.03
K(FC)	3.80	1.25	0.29	0

their total valance charge, respectively while at HC concentration, K transfer 20% of its total valance charge for all N-ZGNR cases. Correspondingly, increase in total valance charge of each edge carbon atom for all N-ZGNR cases are given in tables 5.3-5.4. However at FC concentration K atom gains extra 25% of its valance charge from ZGNR.

5.2.4. Transport Properties

Transmission calculations are performed for the perfect HC concentration of Na termination the 9ZGNR (see Fig 5.12 (b)) and single Na vacancy with HC concentration of Na termination the 9ZGNR (see Figure 5.12 (c)). Also HC concentration of Na termination the 9ZGNR is used as electrodes for both sides (see Figure 5.12 (c)).

Self energies of electrodes are calculated separately and included into the current

Table 5.4. Total valance charge and the spin magnetic moments of the Li, Na, K at HC with 5ZGNR, 6ZGNR, 7ZGNR, 8ZGNR.

	Total Charges		**Magnetic Moments (μ_B)**	
	Edge C	**Adatom**	**Edge C**	**Adatom**
Pristine(5ZGNR)	4.06	-	1.21	-
Li(5ZGNR)	4.12	0.90	0.12	0.03
Na(5ZGNR)	4.14	0.89	0.13	0
K(5ZGNR)	4.17	0.79	0.19	0.03
Pristine(6ZGNR)	4.06	-	1.21	-
Li(6ZGNR)	4.12	0.90	0.11	0.03
Na(6ZGNR)	4.14	0.89	0.13	0
K(6ZGNR)	4.17	0.80	0.14	0.02
Pristine(7ZGNR)	4.06	-	1.21	-
Li(7ZGNR)	4.12	0.90	0.11	0.03
Na(7ZGNR)	4.14	0.89	0.13	0
K(7ZGNR)	4.17	0.80	0.17	0.03
Pristine(8ZGNR)	4.06	-	1.21	-
Li(8ZGNR)	4.12	0.90	0.11	0.03
Na(8ZGNR)	4.14	0.89	0.13	0
K(8ZGNR)	4.17	0.80	0.17	0.03

calculation. Some portion of the electrodes are included into the systems from both sides due to avoid direct interactions between the electrodes they form scattering regions. Geometric optimization of the scattering regions for the both perfect HC concentration of Na termination the 9ZGNR and single Na vacancy with HC concentration of Na termination the 9ZGNR are performed.

During the calculation of the transmission, in order to match the device potential and the surface potential of the semi-infinite electrodes, additionally some more portion of the electrodes are included into the device region. These additionally included parts of the electrodes are kept fixed during the geometric optimizations of the large supercells of scattering regions.

Transmission results under zero bias for perfect and single sodium vacancy cases are given in Figure 5.13. At the left side of the figure spin degenerate transmission plot is displayed for perfect case. Spin polarized current is not expected for an applied small bias at low temperatures for perfect case which it can be calculated from Equation 3.57. Also at the right of the figure the transmission plot is given for single atom vacancy case. In contrary to the perfect case, strong spin polarized current is expected for an applied small bias at low temperatures.

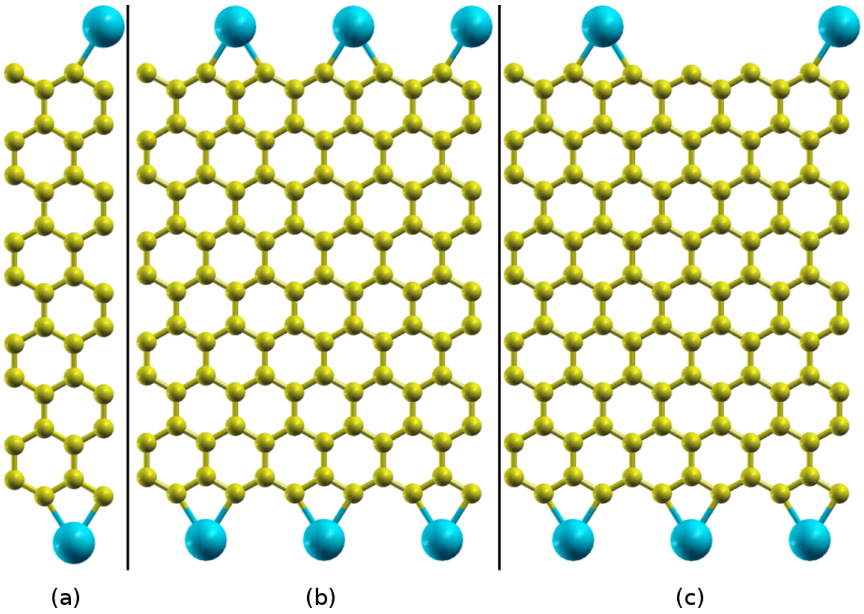

Figure 5.12. (a) Unit cell of the electrodes. (b) Scattering region for perfect HC concentration of Na termination the 9ZGNR. (c) Scattering region for single Na vacancy with HC concentration of Na termination the 9ZGNR.

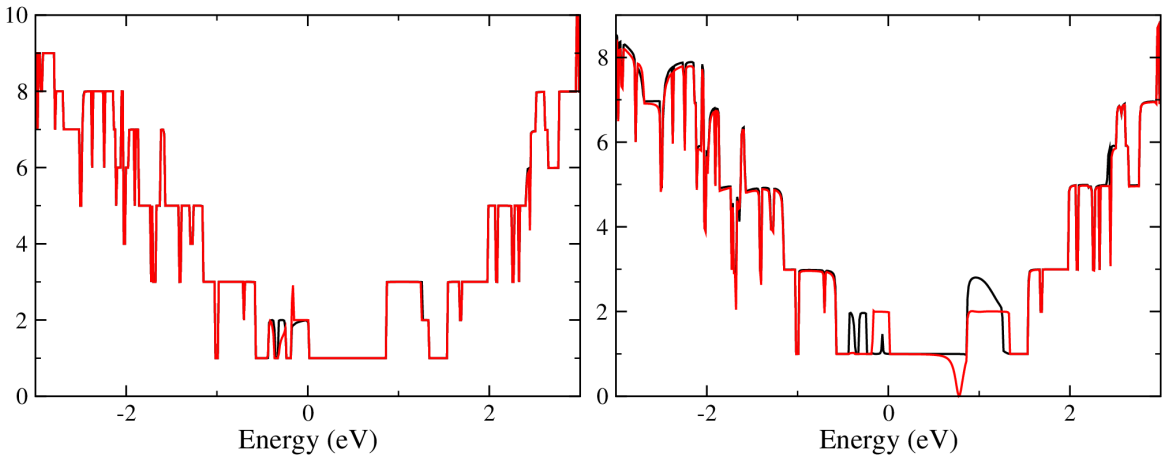

Figure 5.13. (a)Transmission calculation results for perfect HC concentration of Na termination the 9ZGNR. (b) single Na vacancy with HC concentration of Na termination the 9ZGNR. Fermi level is shifted to 0 for both cases.

CHAPTER 6

ADATOM ADSORPTION ON A ONE-DIMENSIONAL TOPOLOGICAL DEFECT IN GRAPHENE

Producing extended defects into the graphene sheet is an alternative approach for the manipulation of electronic properties graphene sheet. Until the recently the only experimentally realized extended defects so far have been the edges of graphene nanoribbons. A recent study on producing one-dimensional topological defect in graphene, containing octagonal and pentagonal sp^2-hybridized carbon rings embedded in a perfect graphene sheet is realized experimentally [149]. The defect which it is produced in graphene acts as a quasi-one-dimensional metallic wire. In this context, adatom adsorption on this one-dimensional topological defect in graphene with large family of adatoms are studied for possible novel electronic, magnetic and spintronic properties.

6.1. Method

First principles density functional theory calculations are carried out using norm-conserving pseudopotentials in their fully nonlocal form and the PBE GGA functional within the SIESTA software package. A double-ζ polarized (a double-ζ for V case) basis set composed of numerical atomic orbitals of finite range. Convergence tests are performed for k-point sampling scheme and mesh cutoff energy. The electrostatic potentials were determined on a real-space grid with a mesh cutoff energy of 350 Ry. The Brillouin zone has been sampled with (1,3,13) points within the Monkhorst-Pack k-point sampling scheme. For geometry optimizations, a local relaxation has been performed using the conjugate gradient algorithm and the convergence criteria of 0.04 eV$\times$Å^{-1} and 10^{-4} eV for the forces and total energies, respectively, in the self-consistency cycles. 5-8 defects are chosen at graphene sheets in z-direction. However even nanowire's unit cell's periodicity is established in z-direction, unit cell is chosen to be periodic at y-direction with enough distance to avoid interactions between 5-8 defect sites in y-direction due to decrease calculation times. Also vacuum region of $\sim$ 10 Å is used in x-direction.

6.2. Results

6.2.1. Geometric Structure

5-8 defects induced geometry of graphenic lattice's unit cell can be seen in Figure6.1. Three possible lowest energetic binding zones are shown in Figure6.1; these are, M1: in

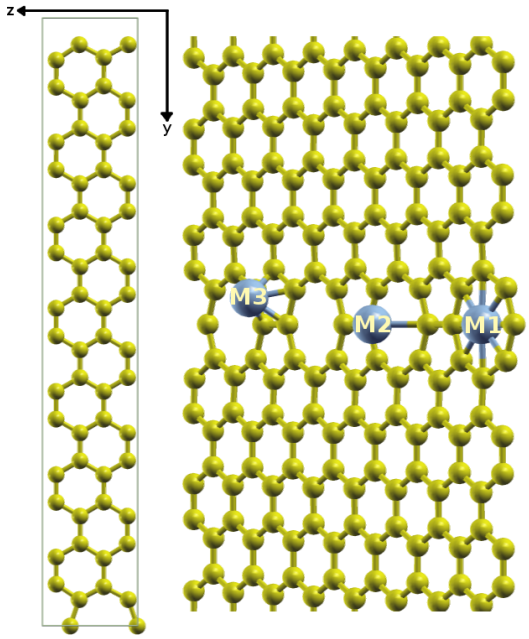

Figure 6.1. Left: Unit cell and geometric structure of 5-8 defect induced graphenic sheet. Right: Possible Binding sites for 5-8 defect induced graphenic sheet.

plane center of the octagon, M2: off plane center of the octagon, M3: off plane center of the pentagon. Firstly, M1 and M2 sites are used as binding zones for Li, Na, Co, Mn, Cr, Ni, Fe, and V atoms. The Li, Na, Co, Mn, Cr, and V atoms are bonded into M1 and M2 zones without deforming the plane geometry of the graphenic sheet, while Ni and Fe atoms are bonded into M1 and M2 zone with deforming the graphenic sheet. Therefore only Li, Na, Co, Mn, Cr, and V atoms are considered for calculations of the electronic and magnetic properties. After the geometry optimizations, Li, Na, Co, Mn, Cr, and V are placed into these M1, M2 binding sites. The lowest energetic geometry was M2 for Li, Na, Co, Mn, Cr, and V atoms in between the M1 and M2 sites.

Unit cell relaxation is performed for Li, Na, Co, Mn, Cr, and V atom adsorption into 5-8 defects induced graphenic sheets. Bond lengths of the three nearest carbon atoms with adatoms and the binding energy for Li, Na, Co, Mn, Cr, and V atoms adsorption into

Table 6.1. Bond lengths and total energies versus different adatoms absorbed into M2 sites of the 5-8 defect induced graphenic sheets.

System Name	C_1-Adatom Bond Length (Å)	C_2-Adatom Bond Length (Å)	C_3-Adatom Bond Length (Å)	Binding Energy (eV)
Li	2.18	2.27	2.41	11.076855
Na	2.47	2.55	2.67	10.255631
V	2.25	2.34	2.45	12.057048
Cr	2.42	2.52	2.67	10.524221
Mn	2.51	2.64	2.77	10.576678
Co	2.15	2.27	2.41	11.870403

M2 sites of the 5-8 defect induced graphenic sheets are given in table 6.1. Binding energy is defined as,

$$E_B = |E_{tot} - E_{pri} - (n \cdot E_{atom})|/n \tag{6.1}$$

where E_{tot} is total energy of the adatom atom adsorbed into 5-8 defects induced graphenic sheet, E_{pri} is total energy of the pristine 5-8 defects induced graphenic sheet, E_{atom} is the total energy energy of the adatom atom only and n is the total number of adatoms atoms in the unit cell. Also for V atom all possible binding sites are considered. Three lowest binding energies are obtained lowest to the highest M1, M3, M2, respectively for V adsorption into defects induced graphenic sheet. Binding energy of the M2 site is 1.382 eV greater then the binding energy of the M1 site for V adsorption into defects induced graphenic sheet.

6.2.2. Electronic Properties

Figure 6.2 represents the energy band and DOS diagrams of the pristine 5-8 defects induced graphenic sheet. 5-8 defects induced graphenic sheet's energy band diagram displays a metallic band structure with spin degeneracy. Figures 6.3-6.5 represent the energy band and DOS diagrams for adatoms adsorption into the 5-8 defects induced graphenic sheets. Alkali atoms, Li and Na, adsorption into the 5-8 defects induced graphenic sheets, slightly changes the energy band diagram of the pristine 5-8 defects induced graphenic sheets. As it can be seen in Figure 6.3 and 6.4, pristine 5-8 defects induced graphenic sheet's bands around Fermi level are slightly shifting into lower energies in both Li and Na adsorption cases due to the electron transfer from Li and Na

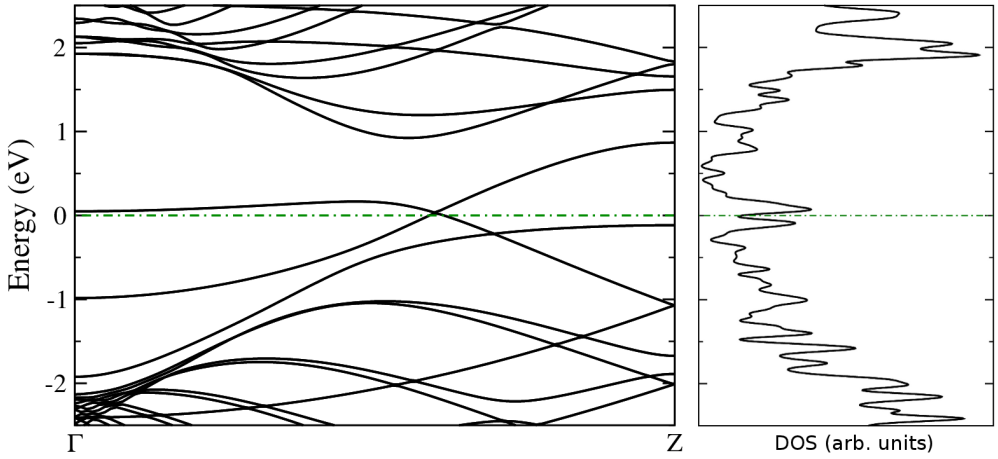

Figure 6.2. Energy band diagram and DOS plot of pristine 5-8 defect induced graphenic sheet. Fermi level is shifted to 0.

into the graphenic sheets. Transition metal atoms, V, Cr, Mn, Co adsorption into the

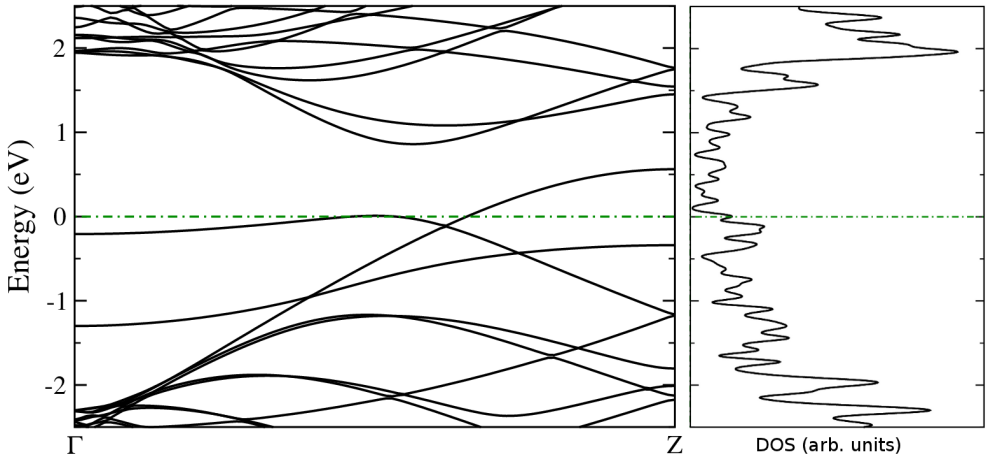

Figure 6.3. Energy band diagram and DOS plot of Li adsorption into the 5-8 defect induced graphenic sheet. Fermi level is shifted to 0.

5-8 defects induced grahpenic sheets, causes spin non-degenerate and different band diagrams (see Figure 6.6-6.5, respectively) . Especially in Figure 6.5, V adsorption into the 5-8 defects induced graphenic sheets change the energy band diagram as half-metallic. For majority spin component the valance and conduction bands intersect at a single point which it is located at $k_0 = 0.416$ in first Brillouin zone ($k_z = 0.634$) while there is no band of the other spin component crossing Fermi level which resulting a energy band gap of 0.7494 eV. The van-Hove singularities are present in the DOS plots of pristine and adatom adsorption into the 5-8 defects induced graphenic sheets which characteristic to one-dimensional systems (see Figure 6.2-6.8). The DOS plots of the transition metals adsorption into the 5-8 defects induced graphenic sheet displays spin-non degenerate DOS

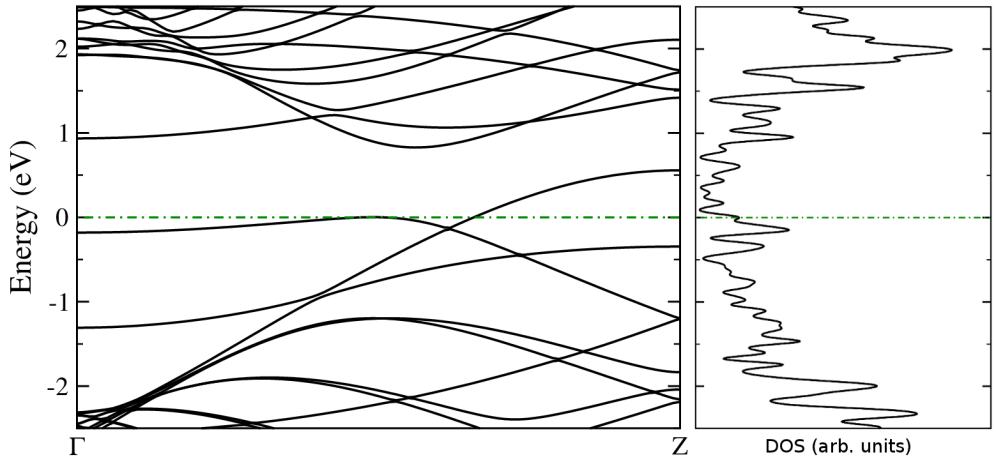

Figure 6.4. Energy band diagram and DOS plot of Na adsorption into the 5-8 defect induced graphenic sheet. Fermi level is shifted to 0.

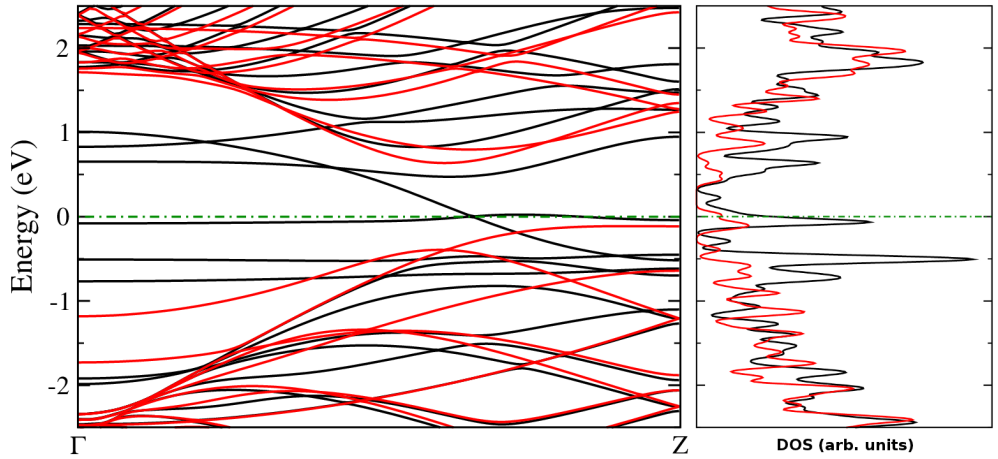

Figure 6.5. Energy band diagram and DOS plot of V adsorption into the 5-8 defect induced graphenic sheet. Fermi level is shifted to 0.

curves (see Figure 6.5 and Fig 6.8). Especially in the V adsorption into the 5-8 defects induced graphenic sheet case, the energy band gap for the majority spin channel is present as expected while minority spin component of density is not vanishing at Fermi level. In contrary to transition metal adsorption into the 5-8 defects induced graphenic sheets, the pristine and Li, Na adsorption into the the 5-8 defects induced graphenic sheets display spin degenerate DOS curves with not vanishing DOS at Fermi level (see Figure 6.2 and Fig 6.4).

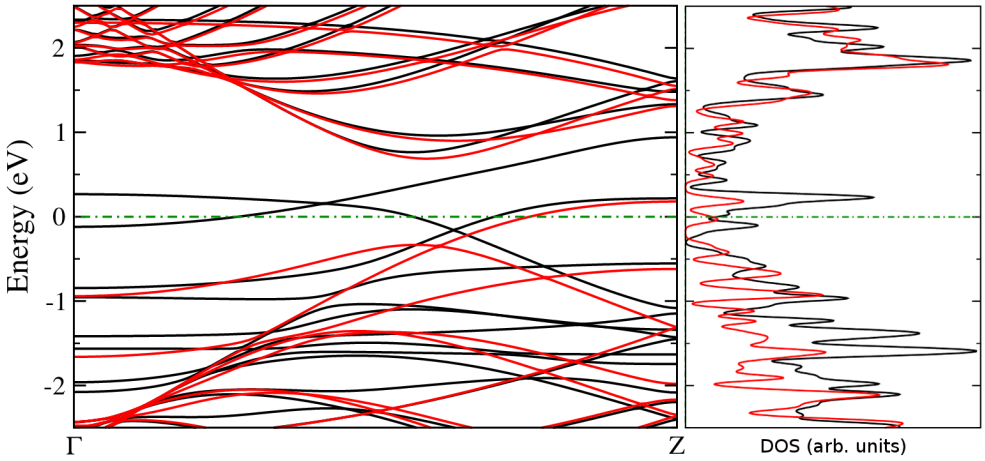

Figure 6.6. Energy band diagram and DOS plot of Cr adsorption into the 5-8 defect induced graphenic sheet. Fermi level is shifted to 0.

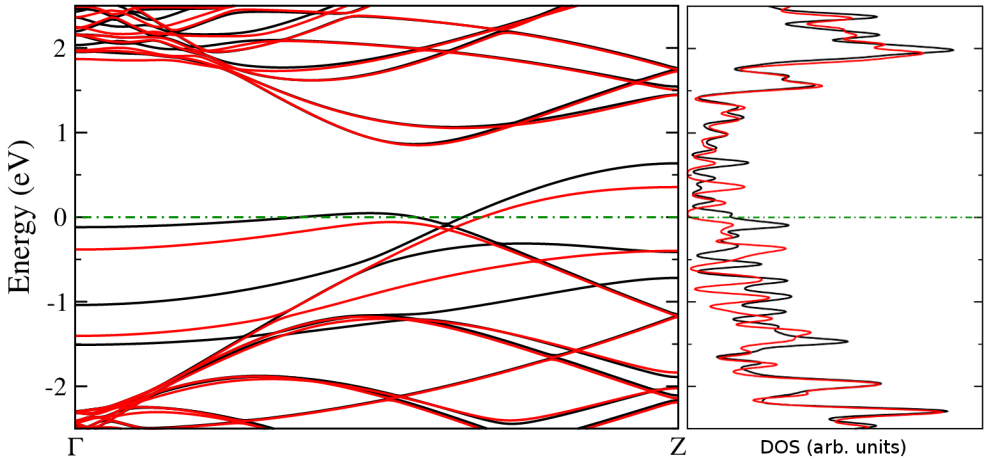

Figure 6.7. Energy band diagram and DOS plot of Mn adsorption into the 5-8 defect induced graphenic sheet. Fermi level is shifted to 0.

6.2.3. Magnetic Properties

The spin-dependent charge densities of the optimized structures and their difference ($\Delta\rho = \rho_{\uparrow} - \rho_{\downarrow}$) are calculated. Using Mulliken population analysis spin dependent atomic charges, total valance charge and the spin magnetic moments of the atoms are determined. Total magnetic moments, total charge of the atoms, and induced magnetic moments of the atoms for adatom adsorption into the 5-8 defects induced graphenic sheets are given in table 6.2. As seen in the table 6.2, there are no net induced magnetic moments on the Li and Na atoms in the Li and Na atoms adsorption into the 5-8 defects induced graphenic sheets. However when one of the Co, Cr, Mn, and V atoms is absorbed into the 5-8 defects induced graphenic sheet, spin magnetic moments are induced

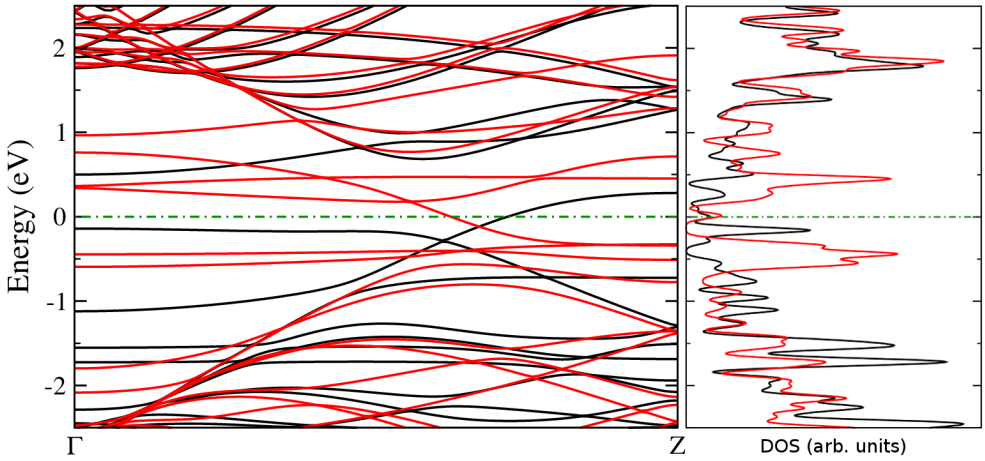

Figure 6.8. Energy band diagram and DOS plot of Co adsorption into the 5-8 defect induced graphenic sheet. Fermi level is shifted to 0.

Table 6.2. Total valance charge and the spin magnetic moments of the octagon C atoms and adatoms for adatom adsorption into the 5-8 defects induced graphenic sheets.

	Li	**Na**	**V**	**Cr**	**Mn**	**Co**
Magnetic Moment (μ_B)	0	0	3.650	5.103	5.954	1.954
Total Charge	0.556	0.59	4.758	5.801	6.556	8.836

on the C atoms of the octagons and adatoms (see Figure 6.9). Especially at the V adsorption into the 5-8 defects induced graphenic sheet case, V atoms induce net magnetic moments on the all of C atoms of the octagons (see Figure 6.9). Also the directions of the spin magnetic moments of the C atoms of octagons are opposite to the direction of the spin magnetic moment of the transition metal atom in Co adsorption into the 5-8 defects induced graphenic sheet case (see Figure 6.9). In Mn adsorption into the 5-8 defects induced graphenic sheet case, Mn atom induces very small spin magnetic moments on the C atoms of the octagons (see Figure 6.9). When an adatom binds to 5-8 defects induced graphenic sheet, the valance charges of the adatoms are partially transferred to the 5-8 defects induced graphenic sheets. Transferred total charges per adatom to the 5-8 defects induced graphenic sheets are 0.136, 0.199, 0.41, 0.444, 0.444, 0.242 for Co, Cr, Na, Li, Mn, V respectively.

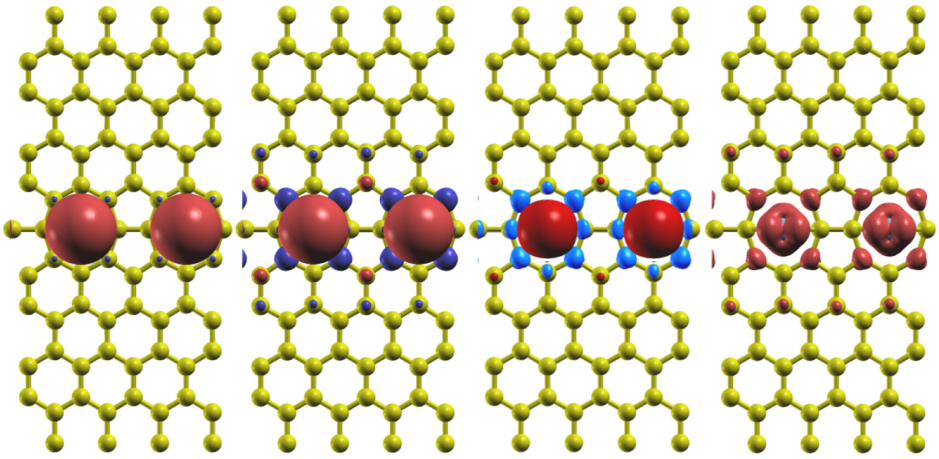

Figure 6.9. Relaxed geometric structure and isosurfaces of charge density difference of spin-up (↑) and spin-down (↓) states for (left to right) Mn, Cr, V, and Co atoms adsorption into the 5-8 defects induced graphenic sheets. For Mn, Cr, Co cases, positive and negative values of the charge density difference is shown by red (dark) and blue (light) regions, respectively, for the same isosurface value of ± 0.004 electrons/Å^3, while for V case, it is ± 0.005 electrons/Å^3.

6.2.4. Transport Properties

Transmission calculations are performed for the following cases: (1) A small part of the pristine 5-8 defects induced graphenic sheet (see Figure 6.10 (b)); (2) one V atom absorbed into the a small part of the 5-8 defects induced graphenic sheet(see Figure 6.10 (c)); (3) and two V atom absorbed into the a small part of the 5-8 defects induced graphenic sheet (see Figure 6.10 (d)). One dimensional pristine 5-8 defects induced graphenic sheets are used as electrodes (see Figure 6.10 (a)) . Self energies of electrodes are calculated separately and included into the current calculation. Some portion of the electrodes are included into the systems from both sides due to avoid direct interactions between the electrodes they form scattering regions .

Geometric optimization of the scattering regions for the two V atom absorbed into the a small part of the 5-8 defects induced graphenic sheet is performed with two different initial spin magnetic moment ordering which they are antiferromagnetic and ferromagnetic. Ferromagnetic ordering for the two V atom absorbed into the a small part of the 5-8 defects induced graphenic sheet has a 0.06 eV lower total energy then antiferromagnetic ordering for the two V atom absorbed into the a small part of the 5-8 defects induced graphenic sheet. In this context two V atom absorbed into the a small part of the 5-8 defects induced graphenic sheet with ferromagnetic ordering is used for transmission calculations.

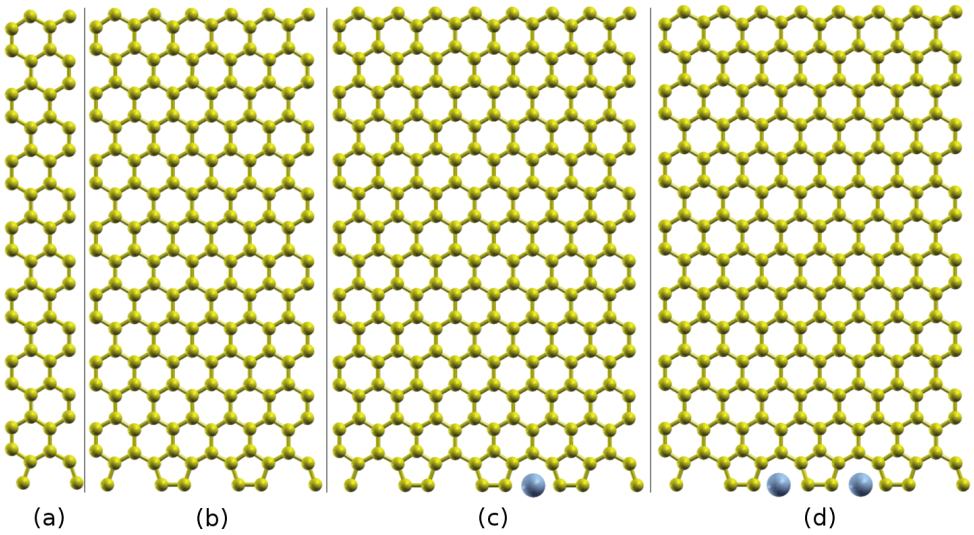

Figure 6.10. (a) Unit cell of the electrodes. (b) Scattering region for a small part of the pristine 5-8 defects induced graphenic sheet. (c) Scattering region for one V atom absorbed into the a small part of the 5-8 defects induced graphenic sheet. (d) Scattering region for two V atom absorbed into the a small part of the 5-8 defects induced graphenic sheet.

During the calculation of the transmission, in order to match the device potential and the surface potential of the semi-infinite electrodes, additionally some more portion of the electrodes are included into the device region. These additionally included parts of the electrodes are kept fixed during the geometric optimizations of the large supercells of scattering regions.

Transmission result under zero bias for pristine 5-8 defects induced graphenic sheet is given in Figure 6.11. In the figure a spin-degenerate transmission plot is displayed. Thus spin polarized current is not expected under low bias and at low temperatures. In the Figure 6.12, transmission results under zero bias for single vanadium and double vanadium adsorption cases are given. At the left side of the figure, transmission plot is given for single vanadium adsorption case. As it can be seen from the figure, under applied small bias and at low temperatures, weak spin polarized current is expected from the Equation 3.57. At the right side of the figure, transmission plot is displayed for double vanadium adsorption case. Using the Equation 3.57 at low temperatures and under small applied bias, very strong spin polarized current is expected in double vanadium adsorption case in contrary to the single vanadium adsorption case.

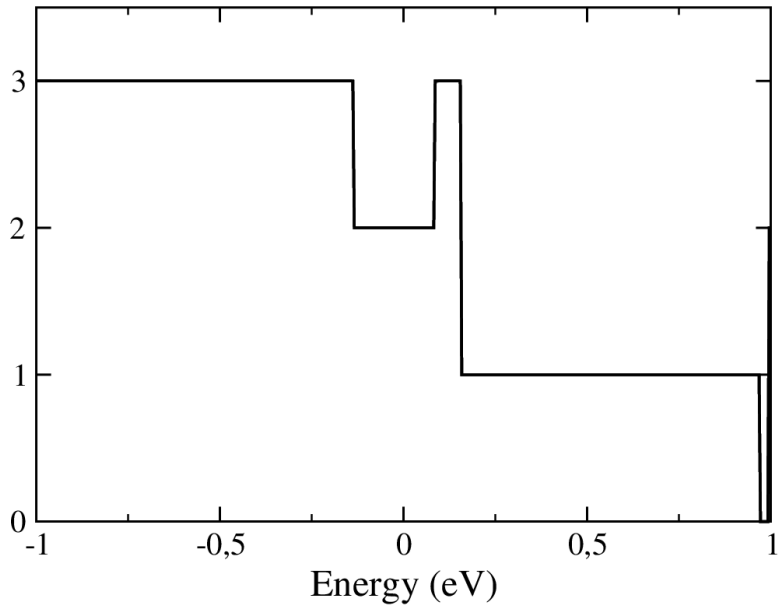

Figure 6.11. Transmission calculation results for a small part of the pristine 5-8 defects induced graphenic sheet. Spin degenerate case. Fermi level shifted to the 0.

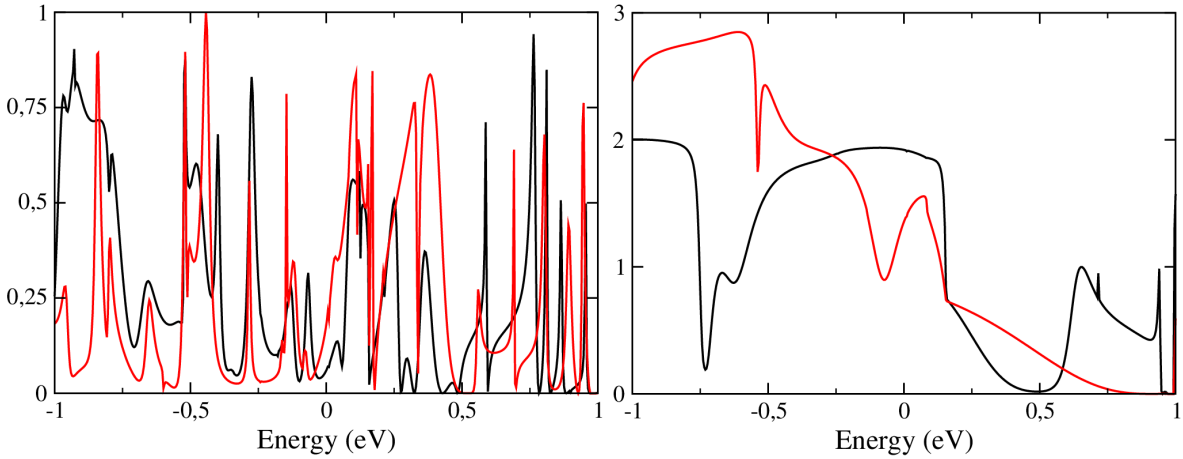

Figure 6.12. Transmission calculation results for V absorbed into the a small part of the 5-8 defects induced graphenic sheet. Left: Absorption of one V atom. Right: Absorption of two V atoms.

CHAPTER 7

CONCLUSIONS

Electronic, spintronic, and transport properties of different examples of nanowires are investigated in this thesis. As first system as nanowire, Cobalt-Benzene nanowire is studied. Different geometric structures of the Cobalt-Benzene nanowires are studied in this thesis which are : (1) Not staggered and antiferromagnetic; (2) Not staggered and ferromagnetic; (3) Staggered and antiferromagnetic; (4) Staggered and ferromagnetic. These systems' geometries are perfectly optimized.

The not staggered and ferromagnetic system has the lowest energy which it becomes the ground state with a very little energy difference with respect to others. Magnitude of the magnetic moments on the Co atoms are 1/3 of the bare Co atom for the not staggered and ferromagnetic case. Also the not staggered and ferromagnetic system's electron band structure diagram and dos plot shows the half-metallic behavior which gives the signal for the possible spintronic properties. In this context, spin polarized current calculation results indicates the only one spin component of the current is dominant for all the range of applied bias window. This makes the not staggered and ferromagnetic system a promising spintronic material especially for the spin polarized current carrying wires.

The antiferromagnetic systems with not staggered and staggered geometries exhibit similar electronic, magnetic and transport properties. Magnitude of the magnetic moments on the Co atoms are 1/4 of the bare Co atom for both not staggered and staggered case with antiferromagnetic ordering. The antiferromagnetic systems display spin degenerate electronic band diagrams and dos plots. However their spin polarized current calculations give the non-degenerate currents in applied bias window. The results of the spin polarized current calculations of the antiferromagnetic systems indicate that the one of the spin component of current is dominant in a specific applied bias window while the other one of the spin component of current is dominant remaining applied bias window. Therefore the antiferromagnetic systems are possible candidates for the spintronic applications especially for the voltage controlled spin filter.

The staggered and ferromagnetic system's energy has the second lowest total energy. The staggered and ferromagnetic system exhibit a half-metal behavior which it can be seen from the band diagram and dos plot of this system. However after the geometric optimization for the scattering region of the staggered and ferromagnetic system, spin

magnetic moments directions and magnitudes are changed. Thus staggered and ferromagnetic system is became staggered and antiferromagnetic.

In summary, the four systems can be divided into the two groups for the spintronic applications. (1) Spin polarized current carrying wires; not staggered antiferromagnetic system, staggered antiferromagnetic system (2) Voltage controlled spin filter; not staggered and ferromagnetic system.

Secondly alkali-atom terminated zigzag graphene nanoribbon system is studied as nanowire. In all cases edge carbon-alkali atom bond length is not affected by the ribbon width. And in all HC concentration cases binding energy of alkali atom increases with the ribbon width. The magnitude of the magnetic moments of the edge carbon atoms are reduced in all cases. FC concentration of Li and Na reduces the band gap of the bare ZGNR. However half coverage concentrations of Li and K with full coverage concentration of K change the ribbon as metal. As a special case, HC concentration of Na, leads to formation of linear bands crossing at the Fermi level. Such tilted Dirac "cones" in a one dimensional material has not been reported before [150]. Also this Dirac cone like band structure is quite robust with respect to the ribbon width and approximations involved. In single sodium vacancy case, different transmission plots are obtained for majority and minority spin channels. Thus at low temperatures and under low bias, spin polarized current is expected in single sodium vacancy case.

Finally, graphenic sheet with periodic 5-8 defect in one direction is studied. Binding of different adatoms (Li, Na, Cr, Co, Mn, and V) to the 5-8 defects induced graphenic sheets are studied in this thesis. 5-8 defects induced graphenic sheets' plane geometries are kept during the adsorption of the adatoms of Li, Na, Cr, Co, Mn and V. Binding energy of the adatom adsorption into the 5-8 defects induced graphenic sheet is greatest in V case. Charge transfer from adatom to the graphenic sheet is occured in all cases. Also transition metal (Cr, Co, Mn, V) adsorption into the 5-8 defects induced graphenic sheets induces spin magnetic moments on the C atoms of octagons.

In all (Li, Na, Cr, Co, Mn, V) cases electronic structures are modified differently. Also in all cases, systems behave as metal except the vanadium adsorption case. Transition metals modifies spin degenerate electronic structure of 5-8 defects induced graphenic sheets to the spin non-degenerate electronic structure. Especially electronic structure of the V adsorption into M2 sites of 5-8 defects induced graphenic sheets is quite interesting due to half-metallic behavior and formation of linear bands crossing at the Fermi level

which they form a tilted Dirac cone. This band structure is similar to the edge termination of 9ZGNR with Na at HC. This half-metallic and tilted Dirac cone behavior may result to the interesting spintronics applications.

Spin polarized current is not expected at pristine 5-8 defects induced graphenic sheet and single vanadium adsorption case , while strong spin polarized current is expected at double vanadium adsorption case at low temperatures and under small bias.

In all three cases, novel electronic, magnetic, and spintronic properties are obtained. These properties are strongly affected by different geometries, defects and adatom adsorptions.

REFERENCES

[1] G. E. Moore. Cramming more components onto integrated circuits (reprinted from electronics, pg 114-117, april 19, 1965). *Proceedings of the Ieee*, 86(1):82–85, 1998.

[2] S. Lloyd. Ultimate physical limits to computation. *Nature*, 406(6799):1047–1054, 2000.

[3] V. V. Zhirnov, R. K. Cavin, J. A. Hutchby, and G. I. Bourianoff. Limits to binary logic switch scaling - a gedanken model. *Proceedings of the Ieee*, 91(11):1934–1939, 2003.

[4] J. R. Black. Electromigration. *Bulletin of the American Physical Society*, 22(3):360–361, 1977.

[5] J. Kao, S. Narendra, and A. Chandrakasan. Subthreshold leakage modeling and reduction techniques. In *Proceedings of the 2002 IEEE/ACM international conference on Computer-aided design*, pages 141–148. ACM, 2002.

[6] Mark Lundstrom. Applied physics: Enhanced: Moore's law forever? *Science*, 299(5604):210–211, 2003.

[7] J. D. Meindl, Q. Chen, and J. A. Davis. Limits on silicon nanoelectronics for terascale integration. *Science*, 293(5537):2044–2049, 2001.

[8] S. A. Wolf, D. D. Awschalom, R. A. Buhrman, J. M. Daughton, S. von Molnar, M. L. Roukes, A. Y. Chtchelkanova, and D. M. Treger. Spintronics: A spin-based electronics vision for the future. *Science*, 294(5546):1488–1495, 2001.

[9] I. Zutic, J. Fabian, and S. Das Sarma. Spintronics: Fundamentals and applications. *Reviews of Modern Physics*, 76(2):323–410, 2004.

[10] W. Thomson. On the Electro-Dynamic Qualities of Metals:–Effects of Magnetization on the Electric Conductivity of Nickel and of Iron. *Proceedings of the Royal Society of London*, 8:546–550, 1856.

[11] R. Meservey, P. M. Tedrow, and P. Fulde. Magnetic field splitting of quasiparticle states in superconducting aluminum films. *Physical Review Letters*, 25(18):1270–1272, 1970.

[12] M. Julliere. Tunneling between ferromagnetic-films. *Physics Letters A*, 54(3):225–226, 1975.

[13] M. N. Baibich, J. M. Broto, A. Fert, F. N. Vandau, F. Petroff, P. Eitenne, G. Creuzet, A. Friederich, and J. Chazelas. Giant magnetoresistance of (001)fe/(001) cr magnetic superlattices. *Physical Review Letters*, 61(21):2472–2475, 1988.

[14] J. Bass and W. P. Pratt. Current-perpendicular (cpp) magnetoresistance in magnetic metallic multilayers. *Journal of Magnetism and Magnetic Materials*, 200(1-3):274–289, 1999.

[15] G. Binasch, P. Grunberg, F. Saurenbach, and W. Zinn. Enhanced magnetoresistance in layered magnetic-structures with antiferromagnetic interlayer exchange. *Physical Review B*, 39(7):4828–4830, 1989.

[16] W. H. Butler, X. G. Zhang, T. C. Schulthess, and J. M. MacLaren. Spin-dependent tunneling conductance of fe vertical bar mgo vertical bar fe sandwiches. *Physical Review B*, 63(5):054416, 2001.

[17] J. Mathon and A. Umerski. Theory of tunneling magnetoresistance of an epitaxial fe/mgo/fe(001) junction. *Physical Review B*, 63(22):220403, 2001.

[18] D. D. Djayaprawira, K. Tsunekawa, M. Nagai, H. Maehara, S. Yamagata, N. Watanabe, S. Yuasa, Y. Suzuki, and K. Ando. 230tunnel junctions. *Applied Physics Letters*, 86(9):092502, 2005.

[19] W. J. Gallagher and S. S. P. Parkin. Development of the magnetic tunnel junction mram at ibm: From first junctions to a 16-mb mram demonstrator chip. *IBM Journal of Research and Development*, 50(1):5–23, 2006.

[20] Y. K. Kato, R. C. Myers, A. C. Gossard, and D. D. Awschalom. Observation of the spin hall effect in semiconductors. *Science*, 306(5703):1910–1913, 2004.

[21] MI Dyakonov and VI Perel. Possibility of orienting electron spins with current. *Soviet Journal of Experimental and Theoretical Physics Letters*, 13:467, 1971.

[22] M. I. Dyakonov and V. I. Perel. Current-induced spin orientation of electrons in semiconductors. *Physics Letters A*, 35(6):459–460, 1971.

[23] J. E. Hirsch. Spin hall effect. *Physical Review Letters*, 83(9):1834–1837, 1999.

[24] S. F. Zhang. Spin hall effect in the presence of spin diffusion. *Physical Review Letters*, 85(2):393–396, 2000.

[25] S. Murakami, N. Nagaosa, and S. C. Zhang. Dissipationless quantum spin current at room temperature. *Science*, 301(5638):1348–1351, 2003.

[26] J. Sinova, D. Culcer, Q. Niu, N. A. Sinitsyn, T. Jungwirth, and A. H. MacDonald. Universal intrinsic spin hall effect. *Physical Review Letters*, 92(12):126603, 2004.

[27] A. Aviram and M. A. Ratner. Molecular rectifiers. *Chemical Physics Letters*, 29(2):277–283, 1974.

[28] V. J. Langlais, R. R. Schlittler, H. Tang, A. Gourdon, C. Joachim, and J. K. Gimzewski. Spatially resolved tunneling along a molecular wire. *Physical Review Letters*, 83(14):2809–2812, 1999.

[29] C. P. Collier, E. W. Wong, M. Belohradsky, F. M. Raymo, J. F. Stoddart, P. J. Kuekes, R. S. Williams, and J. R. Heath. Electronically configurable molecular-based logic gates. *Science*, 285(5426):391–394, 1999.

[30] H. J. Gao, K. Sohlberg, Z. Q. Xue, H. Y. Chen, S. M. Hou, L. P. Ma, X. W. Fang, S. J. Pang, and S. J. Pennycook. Reversible, nanometer-scale conductance transitions in an organic complex. *Physical Review Letters*, 84(8):1780–1783, 2000.

[31] M. A. Reed, J. Chen, A. M. Rawlett, D. W. Price, and J. M. Tour. Molecular random access memory cell. *Applied Physics Letters*, 78(23):3735–3737, 2001.

[32] R. M. Metzger and M. P. Cava. Rectification by a single molecule of hexadecylquinolinium tricyanoquinodimethanide. *Molecular Electronics: Science and Technol-*

ogy, 852:95–115, 1998.

[33] J. Chen, M. A. Reed, A. M. Rawlett, and J. M. Tour. Large on-off ratios and negative differential resistance in a molecular electronic device. *Science*, 286(5444):1550–1552, 1999.

[34] C. Kergueris, J. P. Bourgoin, S. Palacin, D. Esteve, C. Urbina, M. Magoga, and C. Joachim. Electron transport through a metal-molecule-metal junction. *Physical Review B*, 59(19):12505–12513, 1999.

[35] L. A. Bumm, J. J. Arnold, M. T. Cygan, T. D. Dunbar, T. P. Burgin, L. Jones, D. L. Allara, J. M. Tour, and P. S. Weiss. Are single molecular wires conducting? *Science*, 271(5256):1705–1707, 1996.

[36] X. D. Cui, A. Primak, X. Zarate, J. Tomfohr, O. F. Sankey, A. L. Moore, T. A. Moore, D. Gust, G. Harris, and S. M. Lindsay. Reproducible measurement of single-molecule conductivity. *Science*, 294(5542):571–574, 2001.

[37] C. Dekker. Carbon nanotubes as molecular quantum wires. *Physics Today*, 52(5):22–28, 1999.

[38] H. Park, J. Park, A. K. L. Lim, E. H. Anderson, A. P. Alivisatos, and P. L. McEuen. Nanomechanical oscillations in a single-c-60 transistor. *Nature*, 407(6800):57–60, 2000.

[39] J. H. Schon, H. Meng, and Z. N. Bao. Field-effect modulation of the conductance of single molecules. *Science*, 294(5549):2138–2140, 2001.

[40] K.Y. Tan, K.W. Chan, M. Möttönen, A. Morello, C. Yang, J. Donkelaar, A. Alves, J.M. Pirkkalainen, D.N. Jamieson, R.G. Clark, et al. Transport spectroscopy of single phosphorus donors in a silicon nanoscale transistor. *Nano letters*, 10(1):11–15, 2009.

[41] Alexandre R. Rocha, Victor M. Garcia-suarez, Steve W. Bailey, Colin J. Lambert, Jaime Ferrer, and Stefano Sanvito. Towards molecular spintronics. *Nat Mater*, 4(4):335–339, 2005.

[42] K. Tsukagoshi, B. W. Alphenaar, and H. Ago. Coherent transport of electron spin in a ferromagnetically contacted carbon nanotube. *Nature*, 401(6753):572–574, 1999.

[43] L. E. Hueso, J. M. Pruneda, V. Ferrari, G. Burnell, J. P. Valdes-Herrera, B. D. Simons, P. B. Littlewood, E. Artacho, A. Fert, and N. D. Mathur. Transformation of spin information into large electrical signals using carbon nanotubes. *Nature*, 445(7126):410–413, 2007.

[44] M. Ouyang and D. D. Awschalom. Coherent spin transfer between molecularly bridged quantum dots. *Science*, 301(5636):1074–1078, 2003.

[45] Eldon G. Emberly and George Kirczenow. Molecular spintronics: spin-dependent electron transport in molecular wires. *Chemical Physics*, 281(2-3):311–324, 2002.

[46] Ranjit Pati, Laxmidhar Senapati, Pulikel M. Ajayan, and Saroj K. Nayak. First-principles calculations of spin-polarized electron transport in a molecular wire: Molecular spin valve. *Physical Review B*, 68(10):100407, 2003.

[47] Derek Waldron, Paul Haney, Brian Larade, Allan MacDonald, and Hong Guo. Nonlinear spin current and magnetoresistance of molecular tunnel junctions. *Physical Review Letters*, 96(16):166804, 2006.

[48] P. Hohenberg and W. Kohn. Inhomogeneous electron gas. *Phys. Rev*, 136(3B):B864–B871, 1964.

[49] H. W. Kroto, J. R. Heath, S. C. Obrien, R. F. Curl, and R. E. Smalley. C-60 - buckminsterfullerene. *Nature*, 318(6042):162–163, 1985.

[50] K. S. Novoselov, A. K. Geim, S. V. Morozov, D. Jiang, Y. Zhang, S. V. Dubonos, I. V. Grigorieva, and A. A. Firsov. Electric field effect in atomically thin carbon films. *Science*, 306(5296):666–669, 2004.

[51] LD Landau. On the theory of phase transformations II. *JETP*, 11:627, 1937.

[52] L. D. Landau, E. M. Lifshitz, and L. P. Pitaevskii. *Statistical physics*. Pergamon international library of science, technology, engineering, and social studies. Pergamon Press, Oxford ; New York, 3d rev. and enl. edition, 1980.

[53] R. E. Peierls. Quelques proprietes typiques des corpses solides. *Ann. Inst. Henri Poincare*, 4:177–222, 1935.

[54] RE Peierls. Bemerkungen $\tilde{\text{A}}\frac{1}{4}$ber umwandlungstemperaturen. *Helv. Phys. Acta*, 7:81–83, 1934.

[55] K. S. Novoselov, A. K. Geim, S. V. Morozov, D. Jiang, M. I. Katsnelson, I. V. Grigorieva, S. V. Dubonos, and A. A. Firsov. Two-dimensional gas of massless dirac fermions in graphene. *Nature*, 438(7065):197–200, 2005.

[56] K. S. Novoselov, Z. Jiang, Y. Zhang, S. V. Morozov, H. L. Stormer, U. Zeitler, J. C. Maan, G. S. Boebinger, P. Kim, and A. K. Geim. Room-temperature quantum hall effect in graphene. *Science*, 315(5817):1379, 2007.

[57] M. I. Katsnelson, K. S. Novoselov, and A. K. Geim. Chiral tunnelling and the klein paradox in graphene. *Nature Physics*, 2(9):620–625, 2006.

[58] K. I. Bolotin, K. J. Sikes, J. Hone, H. L. Stormer, and P. Kim. Temperature-dependent transport in suspended graphene. *Physical Review Letters*, 101(9):1079–7114, 2008.

[59] K. I. Bolotin, K. J. Sikes, Z. Jiang, M. Klima, G. Fudenberg, J. Hone, P. Kim, and H. L. Stormer. Ultrahigh electron mobility in suspended graphene. *Solid State Communications*, 146(9-10):351–355, 2008.

[60] D. Huertas-Hernando, F. Guinea, and A. Brataas. Spin relaxation times in disordered graphene. *European Physical Journal-Special Topics*, 148:177–181, 2007.

[61] D. Huertas-Hernando, F. Guinea, and A. Brataas. Spin-orbit coupling in curved graphene, fullerenes, nanotubes, and nanotube caps. *Physical Review B*, 74(15):155426, 2006.

[62] H. Min, J. E. Hill, N. A. Sinitsyn, B. R. Sahu, L. Kleinman, and A. H. MacDonald. Intrinsic and rashba spin-orbit interactions in graphene sheets. *Physical Review B*, 74(16):165310, 2006.

[63] P. A. M. Dirac. *The principles of quantum mechanics*. International series of mono-

graphs on physics. Clarendon Press, Oxford,, 4th edition, 1958.

[64] P.A.M. Dirac. Quantum mechanics of many-electron systems. *Proceedings of the Royal Society of London. Series A*, 123(792):714, 1929.

[65] D. R. Hartree. The wave mechanics of an atom with a non-coulomb central field. part iii. term values and intensities in series in optical spectra. *Mathematical Proceedings of the Cambridge Philosophical Society*, 24(03):426–437, 1928.

[66] W. M. C. Foulkes, L. Mitas, R. J. Needs, and G. Rajagopal. Quantum monte carlo simulations of solids. *Reviews of Modern Physics*, 73(1):33–83, 2001.

[67] P. Ordejón, E. Artacho, and J.M. Soler. Self-consistent order-n density-functional calculations for very large systems. *Physical Review B*, 53(16):10441–10444, 1996.

[68] J. M. Soler, E. Artacho, J. D. Gale, A. Garcia, J. Junquera, P. Ordejon, and D. Sanchez-Portal. The siesta method for ab initio order-n materials simulation. *Journal of Physics-Condensed Matter*, 14(11):2745–2779, 2002.

[69] M. Brandbyge, J. L. Mozos, P. Ordejon, J. Taylor, and K. Stokbro. Density-functional method for nonequilibrium electron transport. *Physical Review B*, 65(16):165401, 2002.

[70] M. Di Ventra, S. T. Pantelides, and N. D. Lang. First-principles calculation of transport properties of a molecular device. *Physical Review Letters*, 84(5):979–982, 2000.

[71] S. H. Ke, H. U. Baranger, and W. T. Yang. Electron transport through molecules: Self-consistent and non-self-consistent approaches. *Physical Review B*, 70(8):085410, 2004.

[72] A. R. Rocha, V. M. Garcia-Suarez, S. Bailey, C. Lambert, J. Ferrer, and S. Sanvito. Spin and molecular electronics in atomically generated orbital landscapes. *Physical Review B*, 73(8):085414, 2006.

[73] J. Taylor, H. Guo, and J. Wang. Ab initio modeling of quantum transport properties of molecular electronic devices. *Physical Review B*, 6324(24):245407, 2001.

[74] E. Artacho, E. Anglada, O. Dieguez, J. D. Gale, A. Garcia, J. Junquera, R. M. Martin, P. Ordejon, J. M. Pruneda, D. Sanchez-Portal, and J. M. Soler. The siesta method; developments and applicability. *Journal of Physics-Condensed Matter*, 20(6):064208, 2008.

[75] J.N. Crain and D.T. Pierce. End states in one-dimensional atom chains. *Science*, 307(5710):703, 2005.

[76] J. Dorantes-Dávila and GM Pastor. Magnetic anisotropy of one-dimensional nanostructures of transition metals. *Physical review letters*, 81(1):208–211, 1998.

[77] P. Gambardella, A. Dallmeyer, K. Maiti, MC Malagoli, W. Eberhardt, K. Kern, and C. Carbone. Ferromagnetism in one-dimensional monatomic metal chains. *Nature*, 416(6878):301–304, 2002.

[78] N. Nilius, TM Wallis, and W. Ho. Development of one-dimensional band structure in artificial gold chains. *Science*, 297(5588):1853, 2002.

[79] R. Rurali and N. Lorente. Metallic and Semimetallic Silicon¡ 100¿ Nanowires. *Physical review letters*, 94(2):26805, 2005.

[80] RT Senger, S. Dag, and S. Ciraci. Chiral single-wall gold nanotubes. *Physical review letters*, 93(19):196807, 2004.

[81] J. Shen, R. Skomski, M. Klaua, H. Jenniches, S.S. Manoharan, and J. Kirschner. Magnetism in one dimension: Fe on Cu (111). *Physical Review B*, 56(5):2340, 1997.

[82] Leo Kouwenhoven. Better control of building blocks for quantum computer. *Science Magazine Daily News*, 2011.

[83] Yong Shi. Miniature energy harvesting technology could power wireless electronics. *Science Magazine Daily News*, 2011.

[84] Norman Sanford. Nanowire field-effect transistors. *National Institute of Standards and Technology*, 2011.

[85] Lyle E. Levine. Fundamentals of deformation. *National Institute of Standards and Technology*, 2011.

[86] E. F. Schubert. Quantum mechanics applied to semiconductor devices lecture notes, 2011.

[87] PR Wallace. The band theory of graphite. *Physical Review*, 71(9):622, 1947.

[88] A.H.C. Neto, F. Guinea, NMR Peres, KS Novoselov, and AK Geim. The electronic properties of graphene. *Reviews of Modern Physics*, 81(1):109, 2009.

[89] NW Ashcroft and ND Mermin. *Solid State Physics: 290*. Harcourt Brace College Publ. Orlando, FL, 1976.

[90] L. Tapasztó, G. Dobrik, P. Lambin, and L.P. Biró. Tailoring the atomic structure of graphene nanoribbons by scanning tunnelling microscope lithography. *Nature Nanotechnology*, 3(7):397–401, 2008.

[91] X. Li, X. Wang, L. Zhang, S. Lee, and H. Dai. Chemically derived, ultrasmooth graphene nanoribbon semiconductors. *Science*, 319(5867):1229, 2008.

[92] A. Yamashiro, Y. Shimoi, K. Harigaya, and K. Wakabayashi. Spin-and charge-polarized states in nanographene ribbons with zigzag edges. *Physical Review B*, 68(19):193410, 2003.

[93] H. Lee, Y.W. Son, N. Park, S. Han, and J. Yu. Magnetic ordering at the edges of graphitic fragments: Magnetic tail interactions between the edge-localized states. *Physical Review B*, 72(17):174431, 2005.

[94] L. Pisani, JA Chan, B. Montanari, and NM Harrison. Electronic structure and magnetic properties of graphitic ribbons. *Physical Review B*, 75(6):064418, 2007.

[95] K. Kusakabe and M. Maruyama. Magnetic nanographite. *Physical Review B*, 67(9):092406, 2003.

[96] V. Barone, O. Hod, and G.E. Scuseria. Electronic structure and stability of semiconducting graphene nanoribbons. *Nano letters*, 6(12):2748–2754, 2006.

[97] M. Fujita, K. Wakabayashi, K. Nakada, and K. Kusakabe. Peculiar localized state at zigzag graphite edge. *Journal of the Physical Society of Japan*, 65(7):1920–1923, 1996.

[98] W. Pauli. Über den Zusammenhang des Abschlusses der Elektronengruppen im Atom mit der Komplexstruktur der Spektren. *Zeitschrift für Physik A Hadrons and Nuclei*, 31(1):765–783, 1925.

[99] E. Fermi. Zur Quantelung des idealen einatomigen Gases. *Zeitschrift für Physik A Hadrons and Nuclei*, 36(11):902–912, 1926.

[100] S.N. Bose. Plancks gesetz und lichtquantenhypothese. *Z. Phys*, 26(3):178, 1924.

[101] A. Einstein. Quantentheorie des idealen einatomigen Gases, Sitzber. *Kgl. Preuss. Akad. Wiss*, pages 261–267, 1924.

[102] W. Heisenberg. Mehrkörperproblem und Resonanz in der Quantenmechanik. *Zeitschrift für Physik A Hadrons and Nuclei*, 38(6):411–426, 1926.

[103] P.A.M. Dirac. On the theory of quantum mechanics. *Proceedings of the Royal Society of London. Series A*, 112(762):661, 1926.

[104] Danny Eric Paul Vanpoucke. *Ab initio study of Pt induced nanowires on Ge(001)*. PhD thesis, University of Twente, 2009.

[105] L.H. Thomas. The calculation of atomic fields. In *Mathematical Proceedings of the Cambridge Philosophical Society*, volume 23, pages 542–548. Cambridge Univ Press, 1927.

[106] E. Fermi. Un metodo statistico per la determinazione di alcune priorieta dell'atome. *Rend. Accad. Naz. Lincei*, 6(602-607):32, 1927.

[107] PAM Dirac. Note on exchange phenomena in the Thomas atom. In *Mathematical Proceedings of the Cambridge Philosophical Society*, volume 26, pages 376–385. Cambridge Univ Press, 1930.

[108] W. Kohn, LJ Sham, et al. Self-consistent equations including exchange and correla-

tion effects. *Phys. Rev*, 140(4A):A1133–A1138, 1965.

[109] RP Feynman. Forces in molecules. *Physical Review*, 56(4):340, 1939.

[110] H. Hellmann. Einfuhrung in die Quantumchemie. *Franz Deutsche, Leipzig*, 1937.

[111] OH Nielsen and R.M. Martin. Stresses in semiconductors: Ab initio calculations on Si, Ge, and GaAs. *Physical Review B*, 32(6):3792, 1985.

[112] OH Nielsen and R.M. Martin. Quantum-mechanical theory of stress and force. *Physical Review B*, 32(6):3780, 1985.

[113] MC Payne, MP Teter, DC Allan, TA Arias, and JD Joannopoulos. Iterative minimization techniques for ab initio total-energy calculations: molecular dynamics and conjugate gradients. *Reviews of Modern Physics*, 64(4):1045–1097, 1992.

[114] J.C. Slater. Atomic shielding constants. *Physical Review*, 36(1):57, 1930.

[115] SF Boys. Electronic wave functions. I. A general method of calculation for the stationary states of any molecular system. *Proceedings of the Royal Society of London. Series A. Mathematical and Physical Sciences*, 200(1063):542, 1950.

[116] R.M. Martin. *Electronic structure: basic theory and practical methods*. Cambridge Univ Pr, 2004.

[117] M.R. Geller and W. Kohn. Theory of generalized Wannier functions for nearly periodic potentials. *Physical Review B*, 48(19):14085, 1993.

[118] L. Genovese, A. Neelov, S. Goedecker, T. Deutsch, S.A. Ghasemi, A. Willand, D. Caliste, O. Zilberberg, M. Rayson, A. Bergman, et al. Daubechies wavelets as a basis set for density functional pseudopotential calculations. *The Journal of chemical physics*, 129:014109, 2008.

[119] D. Sánchez-Portal, P. Ordejón, E. Artacho, and J.M. Soler. Density-functional method for very large systems with LCAO basis sets. *International journal of quantum chemistry*, 65(5):453–461, 1997.

[120] U. Barth and L. Hedin. A local exchange-correlation potential for the spin polarized case. i. *Journal of Physics C: Solid State Physics*, 5:1629, 1972.

[121] D.M. Ceperley and BJ Alder. Ground state of the electron gas by a stochastic method. *Physical Review Letters*, 45(7):566–569, 1980.

[122] J.P. Perdew, JA Chevary, SH Vosko, K.A. Jackson, M.R. Pederson, DJ Singh, and C. Fiolhais. Atoms, molecules, solids, and surfaces: Applications of the generalized gradient approximation for exchange and correlation. *Physical Review B*, 46(11):6671, 1992.

[123] A.D. Becke. Density-functional exchange-energy approximation with correct asymptotic behavior. *Physical Review A*, 38(6):3098, 1988.

[124] J.P. Perdew and Y. Wang. Accurate and simple analytic representation of the electron-gas correlation energy. *Physical Review B*, 45(23):13244, 1992.

[125] J.P. Perdew, K. Burke, and M. Ernzerhof. Generalized gradient approximation made simple. *Physical Review Letters*, 77(18):3865–3868, 1996.

[126] A.D. Becke. A new mixing of Hartree–Fock and local density-functional theories. *The Journal of Chemical Physics*, 98:1372, 1993.

[127] J.P. Perdew, M. Ernzerhof, and K. Burke. Rationale for mixing exact exchange with density functional approximations. *The Journal of chemical physics*, 105:9982, 1996.

[128] A. Görling. Exact treatment of exchange in Kohn-Sham band-structure schemes. *Physical Review B*, 53(11):7024, 1996.

[129] M. Städele, JA Majewski, P. Vogl, and A. Görling. Exact Kohn-Sham exchange potential in semiconductors. *Physical review letters*, 79(11):2089–2092, 1997.

[130] M. Städele, M. Moukara, JA Majewski, P. Vogl, and A. Görling. Exact exchange Kohn-Sham formalism applied to semiconductors. *Physical Review B*, 59(15):10031, 1999.

[131] Ivan Rungger. Quantitative theory for electron transport in nano-devices. *Modeling Nanostructures using Density Functional Theory School*, Lecture Notes, 2009.

[132] V.V. Maslyuk, A. Bagrets, V. Meded, A. Arnold, F. Evers, M. Brandbyge, T. Bredow, and I. Mertig. Organometallic benzene-vanadium wire: A one-dimensional half-metallic ferromagnet. *Physical review letters*, 97(9):97201, 2006.

[133] H.B. Yi, H.M. Lee, and K.S. Kim. Interaction of Benzene with Transition Metal Cations: Theoretical Study of Structures, Energies, and IR Spectra. *Journal of Chemical Theory and Computation*, 5(6):1709–1717, 2009.

[134] D. Gunlycke, J. Li, JW Mintmire, and CT White. Altering low-bias transport in zigzag-edge graphene nanostrips with edge chemistry. *Applied Physics Letters*, 91:112108, 2007.

[135] D. Jiang, B.G. Sumpter, and S. Dai. Unique chemical reactivity of a graphene nanoribbon's zigzag edge. *The Journal of chemical physics*, 126:134701, 2007.

[136] DW Boukhvalov and MI Katsnelson. Chemical functionalization of graphene with defects. *Nano letters*, 8(12):4373–4379, 2008.

[137] TB Martins, RH Miwa, A.J.R. da Silva, and A. Fazzio. Electronic and transport properties of boron-doped graphene nanoribbons. *Physical review letters*, 98(19):196803, 2007.

[138] T.B. Martins, A.J.R. da Silva, R.H. Miwa, and A. Fazzio. σ-and π-Defects at Graphene Nanoribbon Edges: Building Spin Filters. *Nano letters*, 8(8):2293–2298, 2008.

[139] SS Yu, WT Zheng, QB Wen, and Q. Jiang. First principle calculations of the electronic properties of nitrogen-doped carbon nanoribbons with zigzag edges. *Carbon*, 46(3):537–543, 2008.

[140] XH Zheng, I. Rungger, Z. Zeng, and S. Sanvito. Effects induced by single and multiple dopants on the transport properties in zigzag-edged graphene nanoribbons. *Physical Review B*, 80(23):235426, 2009.

[141] VA Rigo, TB Martins, A.J.R. da Silva, A. Fazzio, and RH Miwa. Electronic, structural, and transport properties of Ni-doped graphene nanoribbons. *Physical Review B*, 79(7):075435, 2009.

[142] N. Gorjizadeh, A.A. Farajian, K. Esfarjani, and Y. Kawazoe. Spin and band-gap engineering in doped graphene nanoribbons. *Physical Review B*, 78(15):155427, 2008.

[143] C. Ataca, E. Aktürk, H. Şahin, and S. Ciraci. Adsorption of carbon adatoms to graphene and its nanoribbons. *Journal of Applied Physics*, 109:013704, 2011.

[144] E. Kan, Z. Li, J. Yang, and JG Hou. Half-metallicity in edge-modified zigzag graphene nanoribbons. *Journal of the American Chemical Society*, 130(13):4224–4225, 2008.

[145] Y.W. Son, M.L. Cohen, and S.G. Louie. Half-metallic graphene nanoribbons. *Nature*, 444(7117):347–349, 2006.

[146] Y.W. Son, M.L. Cohen, and S.G. Louie. Energy gaps in graphene nanoribbons. *Physical Review Letters*, 97(21):216803, 2006.

[147] MO Goerbig, J.N. Fuchs, G. Montambaux, and F. Piéchon. Tilted anisotropic dirac cones in quinoid-type graphene and α-(bedt-ttf) $_{-}\{2\}$ i$_{-}\{3\}$. *Physical Review B*, 78(4):045415, 2008.

[148] H. Şahin and R.T. Senger. First-principles calculations of spin-dependent conductance of graphene flakes. *Physical Review B*, 78(20):205423, 2008.

[149] J. Lahiri, Y. Lin, P. Bozkurt, I.I. Oleynik, and M. Batzill. An extended defect in graphene as a metallic wire. *Nature Nanotechnology*, 5(5):326–329, 2010.

[150] C. Zhang X. L. Wang, S. X. Dou. Zero-gap materials for future spintronics, electronics and optics. *NPG Asia Materials*, 2(1):31–38, 2010.